

**Texas A&M University**  
**J. Mike Walker'66 Department of Mechanical Engineering**  
**Turbomachinery Laboratory**  
**Tribology Group**

**ON THE LEAKAGE AND DYNAMIC FORCE COEFFICIENTS OF A  
NOVEL STEPPED SHAFT POCKET DAMPER SEAL:  
EXPERIMENTAL AND CFD MODEL VERIFICATION**

**TRC-SEAL-02-19**

Research Progress Report to the Turbomachinery Research Consortium

by

**Jing Yang**

Research Associate

**Luis San Andrés**

Mast-Childs Chair Professor  
Principal Investigator

**Xueliang Lu**

Research Assistant

May 2019

**TRC Project, TEES # 400124-00131**

## EXECUTIVE SUMMARY

High performance turbomachinery favors annular seals with low leakage and a large damping coefficient for rotor system stability; and pocket damper seals (PDSs), since their invention, demonstrate such favorable characteristics. A PDS has axial blades (ribs) and circumferential partition walls (ridges), producing its unique static and dynamic force performance. To further enhance the damping characteristic and reduce the seal leakage, a novel stepped shaft PDS is hereby disclosed. The invention has a unique arrangement of steps on the rotor surface, each facing an upstream rib in a pocket row. Thus the step and the rib tip form a tight clearance ( $c_1$ ). The rotor surface and the downstream rib tip form a larger clearance ( $c_2$ ). The convergence-divergence variation of cross-section areas along flow direction aids to increase the PDS damping coefficient.

To validate the performance of the novel design, a stepped shaft PDS ( $c_1/c_2 = 0.5$ ) with four axial ribs and eight circumferential pockets is built and tested at the Turbomachinery Laboratory. A comprehensive investigation, experimental and numerical, evaluates the seal leakage and dynamic force coefficients for the stepped shaft PDS, as well as the performance of an identical PDS with a smooth rotor surface ( $c_1/c_2 = 1$ , named uniform clearance PDS). The stepped shaft PDS operates with air at supply pressure ranging from 1.1 bar towards 3.2 bar. The measured leakage for the stepped shaft PDS is 50% of that for the uniform clearance PDS. The computational fluid dynamics (CFD) and bulk flow model (BFM) predicted leakage matches well the test data when  $P_S > 1.9$  bar. For  $P_S = 2.3$  bar, the test damping coefficient  $C$  for the stepped shaft PDS is  $\sim 1.5$  times greater than the one for the uniform clearance PDS. With an increase in  $P_S$ , the stepped shaft PDS shows an even more favorable damping characteristic. When  $P_S$  increases from 2.3 bar to 3.2 bar, the test  $C$  grows  $\sim 2.5$  times. The CFD over estimates  $C$  in comparison to the test data,  $\sim$  at most 29% higher for  $P_S = 3.2$  bar, though capturing the variation trend versus frequency. The BFM under predicts  $C$  for the stepped shaft PDS, indicating the BFM limited applicability. The test data and CFD predictions both demonstrate the superior damping performance of the novel stepped shaft PDS.

## TABLE OF CONTENTS

1. Introduction.....	5
2. A stepped shaft and pocket damper seal assembly .....	8
3. Experimental and numerical techniques for estimation of seal leakage and dynamic force coefficients .....	12
4. Results and discussion .....	17
5. Conclusion .....	26
Acknowledgments.....	27
Nomenclature.....	27
References.....	28
Appendix A: Bulk-flow model prediction for pocket damper seals.....	30

## LIST OF TABLES

Table 1. Geometry and operating conditions of a stepped shaft and a four-rib fully partitioned pocket damper seal assembly.....	11
---	----

## LIST OF FIGURES

Figure 1. (a) Photograph of a uniform clearance eight-rib, eight-pocket damper seal; (b) View of a cross-section plane for a pocket damper seal. ....	5
Figure 2. Photograph of a two-rib, four-pocket damper seal (circa 1996). ....	6
Figure 3. Photograph of a half piece of a four-rib fully partitioned damper seal. Taken from Ref. [10]. ....	7
Figure 4. Views of a cross-section plane for (a) a stepped shaft and pocket damper seal assembly; (b) a prior art stepped labyrinth damper seal from Ref. [22]. ....	9
Figure 5. Stepped shaft and a four-rib fully partitioned pocket damper seal assembly.....	10
Figure 6. (a) Photograph of a four-rib fully partitioned pocket damper seal; (b) Cut view of pocket damper seal. ....	10
Figure 7. A cross-section sketch of the stepped shaft and a four-rib fully partitioned pocket damper seal assembly. All dimension in mm. (Not to scale).....	11
Figure 8. (a) Isometric view of seal vertical test rig; (b) cut view of test seal assembly with lubricant flow path. Taken from Ref. [27]. ....	12
Figure 9. Three-dimensional mesh for a stepped shaft and a four-rib fully partitioned pocket damper seal assembly. (a) Three-dimensional mesh; (b) a cross section view of the mesh; and (c) mesh details around first rib and first step. ....	13
Figure 10. (a) A schematic diagram showing the mesh for a stepped rotor and a smooth seal assembly; (b) A likely severe mesh deformation for a stepped rotor and a smooth seal assembly. ....	14
Figure 11. The mesh separation method for a stepped rotor and a smooth seal assembly (not to scale). ....	15
Figure 12. Rotor center displacement during one period of whirl orbit.....	15
Figure 13. Measured, CFD predicted and BFM predicted (a) leakage [g/s]; and (b) flow factor ( $\phi$ ) $\left[ \text{kg}\sqrt{\text{K}}/(\text{MPa}\cdot\text{m}\cdot\text{s}) \right]$ vs. pressure ratio ( $P_s/P_a$ ) for a uniform clearance pocket damper seal (clearance ratio $c_1/c_2 = 1$ ) and a stepped shaft	

pocket damper seal (clearance ratio  $c_1/c_2 = 0.5$ ). Fully partitioned pocket damper seal,  $L/D = 0.38$ ,  $c_2 = 0.184$  mm, exit pressure  $P_a = 1$  bar..... 18

Figure 14. Test derived, CFD predicted and BFM predicted (a) modified flow factor ( $\phi^*$ ) [ $\text{kg}\sqrt{\text{K}}/(\text{MPa}\cdot\text{m}\cdot\text{s})$ ]; and (b) loss coefficient  $c_d$  vs. pressure ratio ( $P_s/P_a$ ) for a uniform clearance pocket damper seal (clearance ratio  $c_1/c_2 = 1$ ) and a stepped shaft pocket damper seal (clearance ratio  $c_1/c_2 = 0.5$ ). Fully partitioned pocket damper seal,  $L/D = 0.38$ ,  $c_2 = 0.184$  mm, exit pressure  $P_a = 1$  bar. .... 19

Figure 15. CFD and BFM predicted static pressure ratio ( $P/P_a$ ) vs. axial distance ( $Z/L$ ) for a uniform clearance pocket damper seal (clearance ratio  $c_1/c_2 = 1$ ) and a stepped shaft pocket damper seal (clearance ratio  $c_1/c_2 = 0.5$ ). Fully partitioned pocket damper seal,  $L/D = 0.38$ ,  $c_2 = 0.184$  mm, supply pressure  $P_s = 2.3$  bar or 3.2 bar, exit pressure  $P_a = 1$  bar. .... 20

Figure 16. CFD predicted static pressure contours on rotor surface [bar] for a uniform clearance pocket damper seal (clearance ratio  $c_1/c_2 = 1$ ) and a stepped shaft pocket damper seal (clearance ratio  $c_1/c_2 = 0.5$ ). Fully- partitioned pocket damper seal,  $L/D = 0.38$ ,  $c_2 = 0.184$  mm, supply pressure  $P_s = 2.3$  bar, exit pressure  $P_a = 1$  bar..... 21

Figure 17. CFD predicted static pressure contours on stator surface [bar] for a uniform clearance pocket damper seal (clearance ratio  $c_1/c_2 = 1$ ) and a stepped shaft pocket damper seal (clearance ratio  $c_1/c_2 = 0.5$ ). Fully- partitioned pocket damper seal,  $L/D = 0.38$ ,  $c_2 = 0.184$  mm, supply pressure  $P_s = 2.3$  bar, exit pressure  $P_a = 1$  bar..... 21

Figure 18. CFD predicted average axial velocity [m/s] along axial direction ( $Z/L$ ) for a uniform clearance pocket damper seal (clearance ratio  $c_1/c_2 = 1$ ) and a stepped shaft pocket damper seal (clearance ratio  $c_1/c_2 = 0.5$ ). Fully partitioned pocket damper seal,  $L/D = 0.38$ ,  $c_2 = 0.184$  mm, supply pressure  $P_s = 2.3$  bar or 3.2 bar, exit pressure  $P_a = 1$  bar. .... 22

Figure 19. CFD predicted direct dynamic stiffness  $H_R$  and direct damping  $C$  by using a medium mesh (node count  $3.9\times 10^6$ ) and a finer mesh (node count  $5.9\times 10^6$ ) versus excitation frequency  $\omega$  [Hz] for a stepped shaft pocket damper seal (clearance ratio  $c_1/c_2 = 0.5$ ). Fully partitioned pocket damper seal,  $L/D = 0.38$ ,  $c_2 = 0.184$  mm, supply pressure  $P_s = 2.3$  bar, exit pressure  $P_a = 1$  bar. .... 23

Figure 20. Test derived, CFD predicted and BFM predicted direct dynamic stiffness  $H_R$  and direct damping  $C$  versus excitation frequency  $\omega$  [Hz] for a uniform clearance pocket damper seal (clearance ratio  $c_1/c_2 = 1$ ) and a stepped shaft pocket damper seal (clearance ratio  $c_1/c_2 = 0.5$ ). Fully partitioned pocket damper seal,  $L/D = 0.38$ ,  $c_2 = 0.184$  mm, supply pressure  $P_s = 2.3$  bar or 3.2 bar, exit pressure  $P_a = 1$  bar..... 25

Figure 21. Input of geometry and operating fluid properties in PD\_Seal<sup>®</sup>. Stepped shaft pocket damper seal (clearance ratio  $c_1/c_2 = 0.5$ ),  $L/D = 0.38$ ,  $c_2 = 0.184$  mm, supply pressure  $P_s = 2.3$  bar, exit pressure  $P_a = 1$  bar..... 30

Figure 22. Input of operating conditions in PD\_Seal<sup>®</sup>. Stepped shaft pocket damper seal (clearance ratio  $c_1/c_2 = 0.5$ ),  $L/D = 0.38$ ,  $c_2 = 0.184$  mm, supply pressure  $P_s = 2.3$  bar, exit pressure  $P_a = 1$  bar. .... 31

Figure 23. Predicted results in PD\_Seal<sup>®</sup>. Stepped shaft pocket damper seal (clearance ratio  $c_1/c_2 = 0.5$ ),  $L/D = 0.38$ ,  $c_2 = 0.184$  mm, supply pressure  $P_s = 2.3$  bar, exit pressure  $P_a = 1$  bar. .... 31

## 1. INTRODUCTION

Centrifugal compressors and gas turbines often operate above their first critical speed because a high operational shaft speed enables a large power density. During the start up or coast down speed processes, the spinning rotor has to cross one or more critical speeds. If the rotating system does not have enough damping when crossing a critical speed, the rotor vibration may be too large so as to trigger a trip event and an immediate stop mechanism to protect the machine.

Damper seals are frequently utilized as they offer large damping to reduce rotor vibrations in a turbomachinery [1]. One type of damper seal is the pocket damper seal (PDS) [2, 3], shown in Figure 1. In a PDS axial blades (ribs) and circumferential partition walls (ridges) produce a seal unique static and dynamic force performance. The tip of the ribs on the seal stator are very close to the rotor thus forming a small clearance restricting leakage and producing damping. A group of circumferentially positioned partition walls (for instance  $90^\circ$  apart,  $45^\circ$  apart, etc.), namely ridges, separate the annular cavities into several pockets. The depth of the pockets is much larger than the clearance between the rib tips and the rotor.

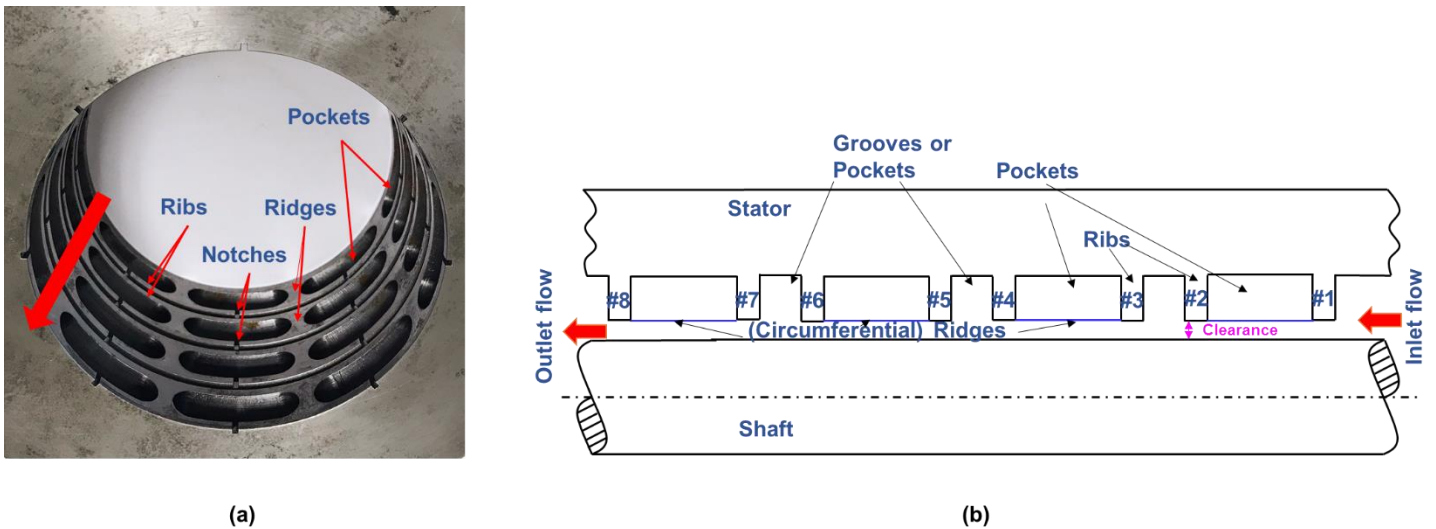
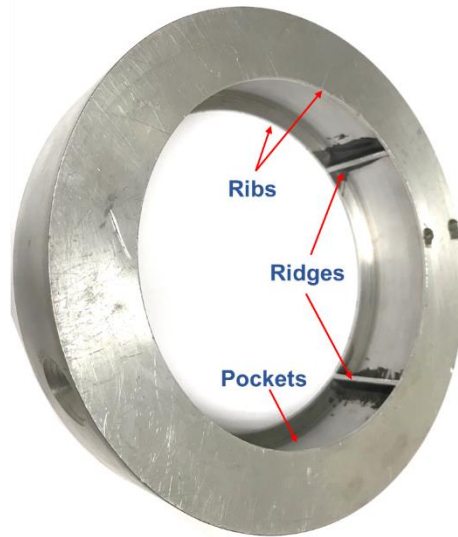


Figure 1. (a) Photograph of a uniform clearance eight-rib, eight-pocket damper seal; (b) View of a cross-section plane for a pocket damper seal.

In 1991, Vance and Shultz [2] invented the PDS, known as TAMSEAL<sup>®</sup>. As shown in Figure 2, this two-rib, four-pocket damper seal derives from adding circumferential ridges in the cavity of a conventional labyrinth seal (LABY), to produce  $\sim 100$  times larger direct damping than the LABY [4]. Note Benckert and Wachter [5] in 1980 also introduced a similar concept, with swirl webs. In 1999, Ransom et al. [6] measure the leakage and dynamic force coefficients of a two-rib, four-pocket damper seal and a LABY of the same dimensions (see

photograph in Figure 2). The supply pressure varies from 1 bar to 3 bar and rotor speed ranges from 1,500 rpm to 3,000 rpm (rotor surface speed from 10 m/s towards 20 m/s). The test data indicates the PDS has a large positive direct damping and a negative direct stiffness, while the LABY shows a negative direct damping and a positive direct stiffness.



**Figure 2. Photograph of a two-rib, four-pocket damper seal (circa 1996).**

A PDS with a divergent clearance is to produce a larger (positive) damping than a similar PDS with a straight clearance does [7]. A simple method to form a divergent clearance and thus increasing damping is introducing notches at the exit (downstream) rib of a pocket [8], as seen in Figure 1 (a). In 2006, Ertas et al. [9] perform experiments to investigate the dynamic performance of four PDSs, incorporating two straight through PDSs with twelve ribs and eight ribs respectively, and two PDSs with downstream notches (of the same dimensions). The four seals operate with supply pressure as high as 69 bar and rotor speed up to 20,200 rpm (rotor surface speed 121 m/s). The PDSs with downstream notches show larger direct damping and less direct stiffness (turning negative), in comparison with the straight through PDSs. The increase in axial rib number, from eight to twelve, produces an increase in the seal direct damping and a reduction in the direct stiffness coefficient.

The above PDSs belong to the conventional type. More recent developments [10, 11] show a fully partitioned damper seal possesses significantly more positive direct damping and direct stiffness than a conventional PDS does. The fully partitioned PDS has radial ridges separating all the cavities into pockets, as shown in Figure 3. In 2002, Li et al. [10] test a fully partitioned PDS and a conventional PDS operating with supply pressure equal to 14.5 bar and rotor speed up to 8,000 rpm (rotor surface speed 41 m/s), demonstrating a fully partitioned PDS does

help to enlarge the rotor critical speed and decrease the motion amplification factor for the rotor system. Later in 2007, Ertas and Vance [11] perform experimental investigations of the dynamic force coefficients for a fully partitioned PDS and a conventional PDS under a large supply pressure (69 bar) and a fast rotor speed (20,200 rpm, rotor surface speed 121 m/s). The test data show the fully partitioned PDS has superior damping performance and larger direct stiffness coefficient than those of the conventional PDS tested under identical operating conditions.

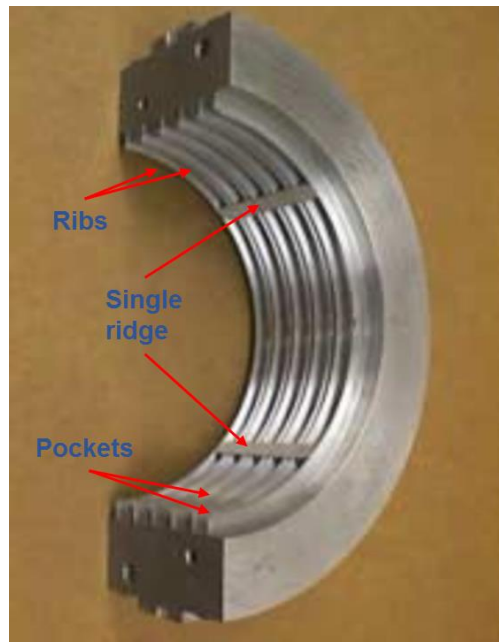


**Figure 3. Photograph of a half piece of a four-rib fully partitioned damper seal. Taken from Ref. [10].**

Numerical methods also aid to the development of PDSs. In 1993, Vance et al. [12] conduct the earliest analysis of a gas pocket damper actuator and predict direct stiffness and direct damping coefficients as functions of the excitation frequency. Later in 1999, Li et al. [13, 14] develop a one-control-volume bulk flow model (BFM) predicting leakage and dynamic force coefficients for PDSs. For a two-rib, four-pocket damper seal [14], the BFM predicted leakage agrees with the test data. The BFM under-estimates the seal direct stiffness coefficient and over-predicts the direct damping coefficient in comparison to those test derived coefficients. In a later prediction (2000) [15] for a four-rib, four-pocket damper seal, the BFM predicted force coefficients deviate from test data yet still with acceptable accuracy per industrial requirements.

Computational fluid dynamics (CFD) plays a significant role in the predictions of static and dynamic performance for PDSs. In 2012, Li et al. [16] develop a CFD approach implementing a multi-frequency, elliptic

orbit whirl model and Fast Fourier Transform to estimate the seal dynamic force coefficients. The CFD predictions for an eight-rib, eight-pocket damper seal match well the test leakage and force coefficients from Ref. [9], demonstrating the accuracy and reliability of the CFD method. Later in 2016, Li et al. [17] employ the CFD method to compare the influences of partition wall type (conventional vs. fully partitioned) on PDS forced performance. The fully partitioned PDS shows larger direct stiffness and direct damping coefficients in comparison with a conventional PDS. Thus, the fully partitioned PDS has superior stability characteristics than a conventional PDS, agreeing with the experimental results in Ref. [11].

Since the invention of the PDS, the Turbomachinery Laboratory at TAMU is at the forefront of its investigation and further development. Recently, an experimental and CFD investigation on a four-rib, eight-pocket fully partitioned damper seal ( $L/D = 0.38$ ,  $C_r = 0.184$  mm) [18], first of its kind, reveals the evolution of the static and dynamic forced performance of a fully portioned PDS operating with a pure gas and also with an oil in air mixture (*wet* gas). The experiments aim to improve PDSs for applications in subsea liquid tolerant compression systems. In comparison to the PDS operating with pure air, the seal experimental dynamic direct stiffness decreases (from positive into negative) when operating with a small amount of oil in air (inlet liquid fraction = 0.4%). With a liquid, both test cross-coupled dynamic stiffness and direct damping show a much larger magnitude than their counterparts for the *dry* gas condition.

To further enhance the damping performance of PDSs and based on prior art and experience, the authors developed an invention: a stepped shaft and PDS assembly<sup>1</sup> [19]. Unlike the above mentioned divergent clearance PDS or a PDS with notches on the stator blades, both costly to fabricate; the stepped shaft PDS is easy to manufacture, whilst still being able to produce significant damping to suppress rotor vibration and maintaining the same or lesser leakage (secondary flow). This report introduces the design concept and details, based on both measurements and CFD analyses, on the superior static and dynamic force performance of the stepped shaft PDS in comparison to a fully portioned PDS of the same dimensions.

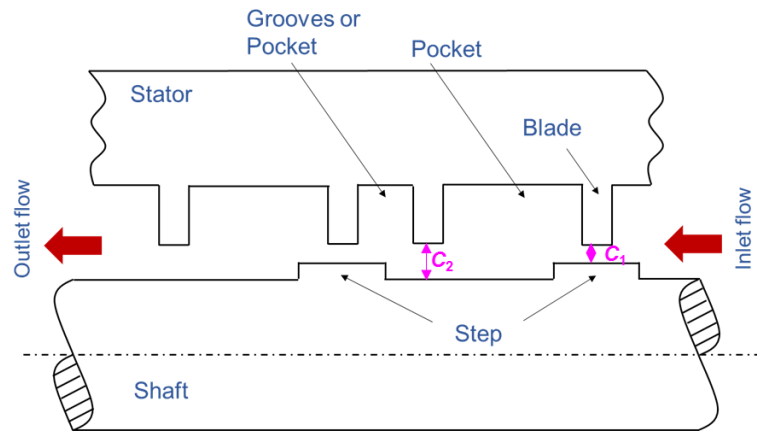
## 2. A STEPPED SHAFT AND POCKET DAMPER SEAL ASSEMBLY

The invention comprises a PDS and a spinning shaft with a stepped surface. Along the axial direction, the PDS contains a plurality ( $N$ ) of pockets separated by ( $N-1$ ) grooves (named as a conventional PDS) or pockets (named as a fully partitioned PDS). As Figure 4(a) shows, the shaft or rotor has a stepped surface facing the upstream rib of a pocket row. In such a way, a step on the rotor surface and the corresponding tip of the rib on the stator form a section with a small clearance (see  $c_1$  in Figure 4(a)). At the exit section of the pocket, the rotor

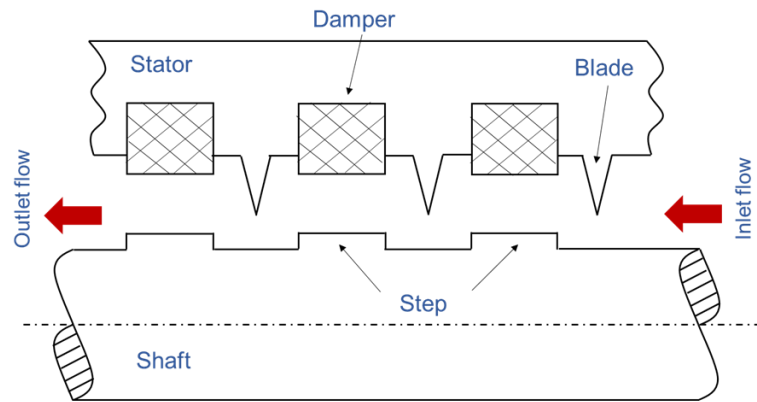
---

<sup>1</sup> Provisional patent No. TAMUS 4990, CR2238-12000 submitted on November 21, 2018.

surface does not have a step, forming a large clearance  $c_2$  ( $c_2 > c_1$ ). The design has a unique arraignment of steps, which is different from the stepped labyrinth seals or hole-pattern seals in Refs. [20-24] whose steps on the rotor face the seal (deep) grooves/pockets/cavities, as shown in Figure 4(b).



(a) The stepped shaft and pocket damper seal assembly



(b) A prior art stepped labyrinth damper seal from Ref. [22]

Figure 4. Views of a cross-section plane for (a) a stepped shaft and pocket damper seal assembly; (b) a prior art stepped labyrinth damper seal from Ref. [22].

To evaluate the leakage and dynamic performance of the novel damper seal, the authors built a four-rib fully partitioned PDS and a stepped shaft assembly shown in Figure 5, and with Figure 6 displaying a photograph and a cut view of the test seal. The PDS has four axial ribs and eight circumferential pockets ( $45^\circ$  apart). Figure 7 depicts a cross-section plane of the stepped shaft PDS. There are two steps on the shaft corresponding to the first and third ribs of the fully partitioned PDS respectively. The clearance ratio for the stepped shaft PDS is presently,  $c_1/c_2 = 0.5$ .

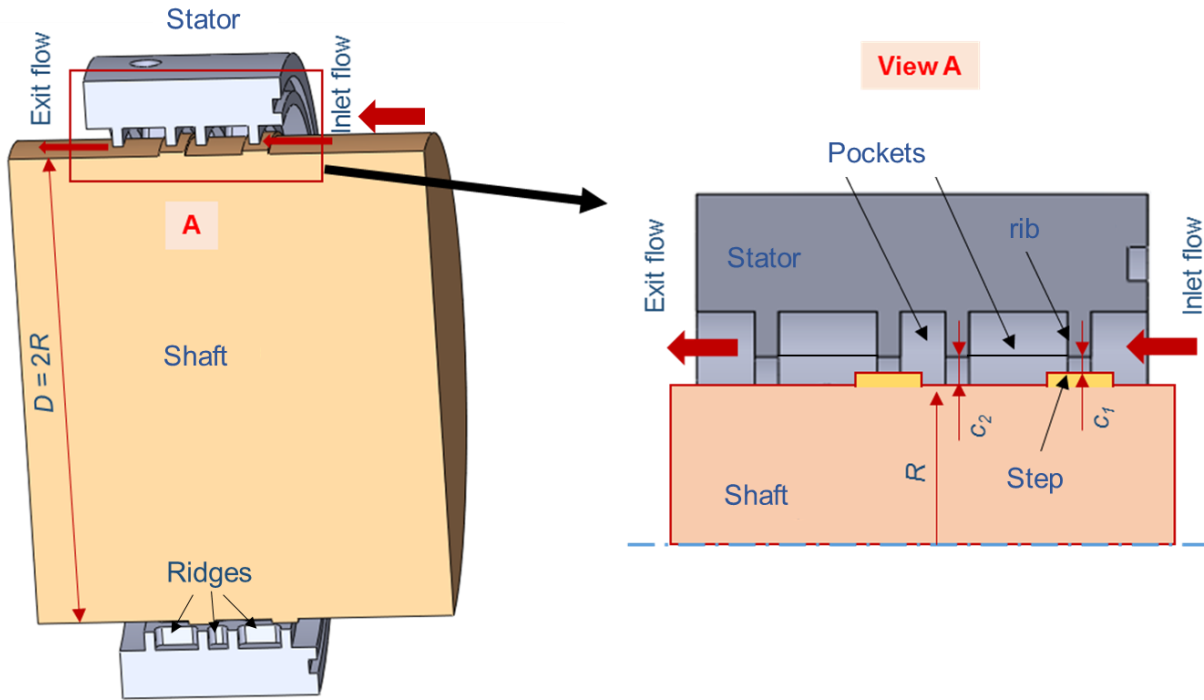


Figure 5. Stepped shaft and a four-rib fully partitioned pocket damper seal assembly.

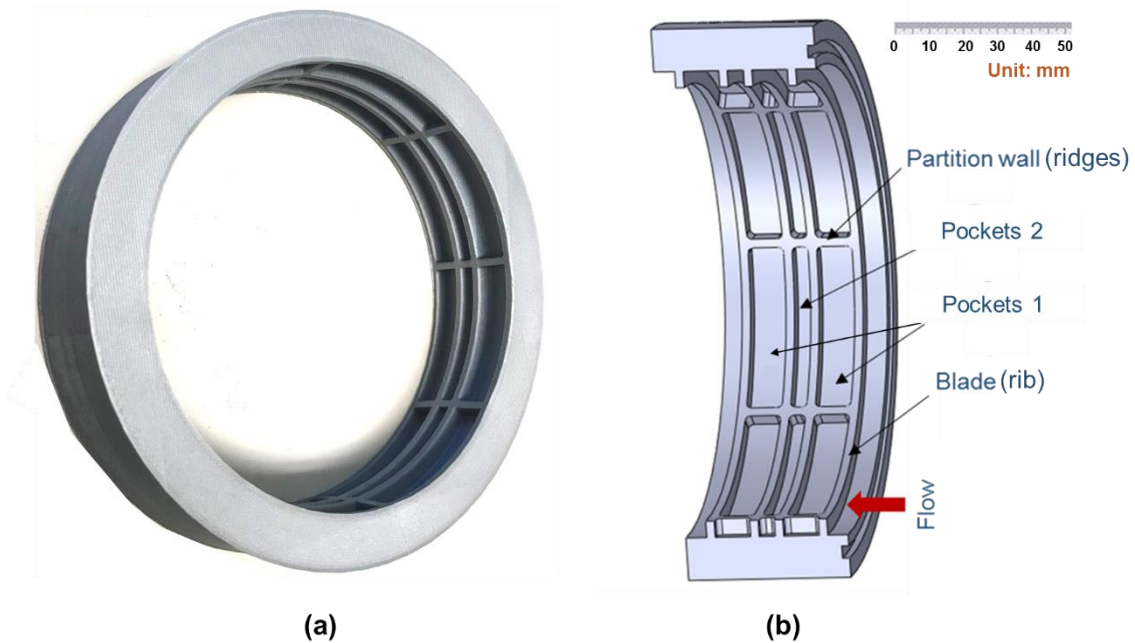
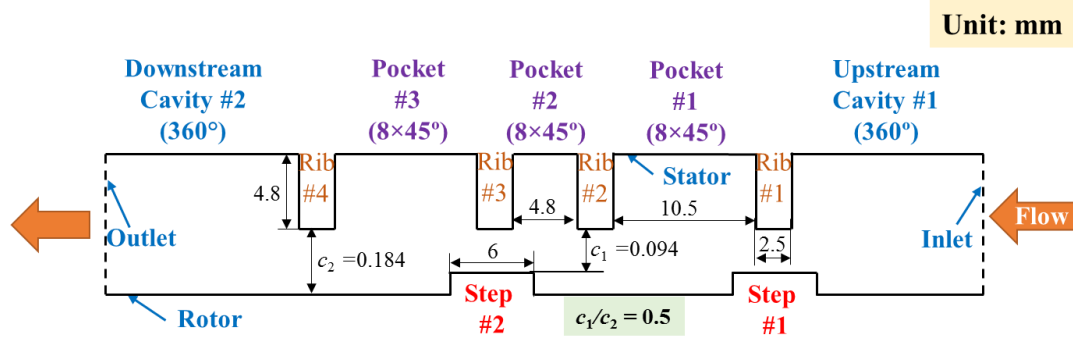


Figure 6. (a) Photograph of a four-rib fully partitioned pocket damper seal; (b) Cut view of pocket damper seal.



**Figure 7. A cross-section sketch of the stepped shaft and a four-rib fully partitioned pocket damper seal assembly. All dimension in mm. (Not to scale)**

Table 1 lists the geometry and operating conditions of the stepped shaft fully partitioned PDS. The step on the shaft and the corresponding tip of the rib upstream of a pocket form a small clearance,  $c_1 = 0.094$  mm. The shaft surface and the rib at the exit section of the pocket make a larger clearance,  $c_2 = 0.184$  mm (step clearance ratio  $c_1/c_2 = 0.5$ ). Note the low supply pressure  $P_s$  (up to 3.2 bar) makes the current PDSs adequate as an inter-stage seal, rather than a balance piston seal. The shaft speed is zero since the current research focuses on seal leakage and damping performance, both known to be independent of rotor speed [25]. A fully partitioned PDS with a smooth surface shaft ( $c_1/c_2 = 1$ ), is also under scrutiny for performance comparisons to the stepped shaft PDS. In the following, the fully partitioned PDS with a smooth surface shaft is simply named uniform clearance PDS.

**Table 1. Geometry and operating conditions of a stepped shaft and a four-rib fully partitioned pocket damper seal assembly.**

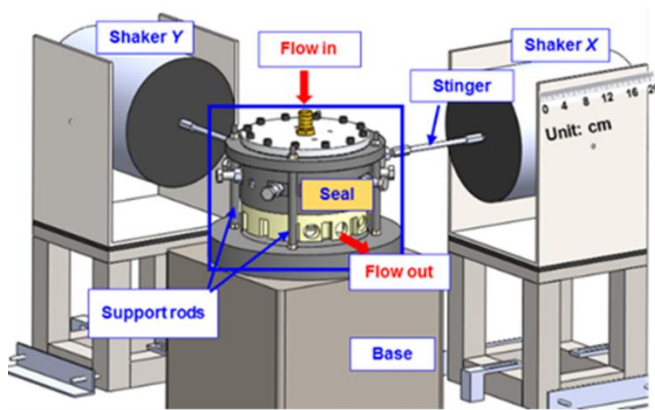
Seal length, $L$	48 mm
Rotor diameter, $D = 2R$	127 mm
Seal radial clearance at a step, $c_1$	0.094 mm
Seal radial clearance, $c_2$	0.184 mm
Number of blades ( <i>ribs</i> )	4 (axial)
Number of partition walls	8 (circumferential)
Cavity length, $L_C$	10.5 mm / 4.8 mm
Cavity depth, $d_C$	4.8 mm
Rib axial thickness, $\delta$	2.5 mm
Step width, $L_{step}$	6 mm
Step height, $d_{step}$	0.09 mm
Working fluid	Air (ideal gas)
Supply pressure, $P_s$	1.1 ~ 3.2 bar
Exit pressure, $P_a$	1 bar
Supply temperature, $T_s$	315 K
Density of fluid at $(P_a, T_s)$ , $\rho_s$	1.11 kg/m <sup>3</sup>
Dynamic viscosity at $(P_a, T_s)$ , $\mu_s$	$1.9 \times 10^{-5}$ kg/(m·s)
Rotor speed	0 rpm

### 3. EXPERIMENTAL AND NUMERICAL TECHNIQUES FOR ESTIMATION OF SEAL LEAKAGE AND DYNAMIC FORCE COEFFICIENTS

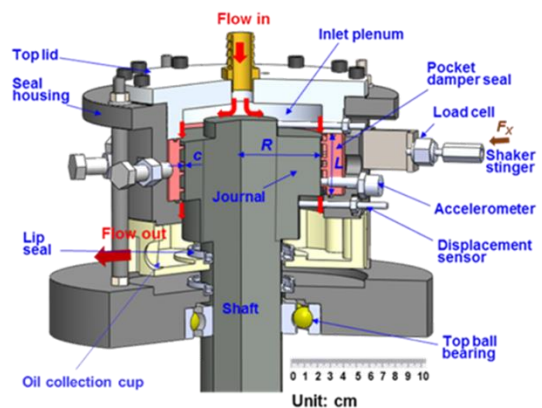
#### Test rig description and experimental procedure

San Andrés et al. [26, 27] describe a test rig to measure the leakage and dynamic force performance of annular pressure seals. The operating fluid can be either air or a two phase flow (oil in air mixture or air in oil mixture). As Figure 8(a) shows, the test rig incorporates a seal housing fixing to a steel base by four support rods, two orthogonal stingers connecting two shakers to the housing, and two flow meters recording the liquid and gas volumetric flow rates. Figure 8(b) displays a cut view of the test seal assembly. During tests, two load cells record the applied loads, four eddy current sensors measure the relative displacements between the housing and the journal, and two accelerometers keep track of the absolute accelerations of the seal housing. A data acquisition system receives the signals from the sensors at a 12,800 samples/second rate.

The test procedure includes three steps. The first step is to identify the test rig structure parameters under a dry condition (operation without supply air). Two shakers apply single frequency loads on the seal housing (20 to 120 Hz, in steps of 10 Hz). Meanwhile the displacement sensors and accelerometers record the transient signals. A frequency domain analysis tool identifies the support structure parameters. The second step is to measure the lubricated system force coefficients (sums of structure parameters and test seal force coefficients). Tests are conducted for a seal operating with a pressurized air. Those measured force coefficients are the lubricated system parameters. The last step is to derive the seal force coefficients through subtracting the structure parameters from the system force coefficients. See Refs. [26, 27] for detailed descriptions of the test rig and test procedure.



(a) Isometric view of seal test rig



(b) Cut view of test seal assembly with lubricant flow path

Figure 8. (a) Isometric view of seal vertical test rig; (b) cut view of test seal assembly with lubricant flow path. Taken from Ref. [27].

## CFD approach

Figure 9 displays the three-dimensional mesh for the stepped shaft and a fully partitioned PDS assembly. The mesh node amount is  $\sim 3.9 \times 10^6$ . A grid independence analysis employs a finer mesh with node count  $\sim 5.9 \times 10^6$ , which will be shown later, proves the medium mesh (node amount  $\sim 3.9 \times 10^6$ ) in present CFD predictions of leakage and dynamic force coefficients are fine enough. Besides the stepped shaft PDS, the CFD analysis also identifies the regular fully partitioned PDS for comparison. The mesh for the regular PDS (node count  $\sim 3.6 \times 10^6$ ) is similar to the stepped shaft PDS. A grid independence analysis against a finer mesh with node count  $\sim 5.7 \times 10^6$  in Ref. [18] already demonstrates its reliability in the CFD predictions, which will not repeat here for brevity. For further details about the mesh for the regular PDS, see Ref. [18].

The commercial CFD software [28] solves the three-dimensional Reynolds-averaged Navier-Stokes equations. The realizable  $k-\varepsilon$  turbulence model with a scalable wall function resolves the turbulent flow through the seals. The supply pressure ( $P_s$ ) and exit pressure ( $P_a$ ) are specified at the seal inlet and outlet respectively. The inlet circumferential velocity equals to zero, in accordance with the experimental setup. The non-slip flow condition applies to the shaft and stator surfaces.

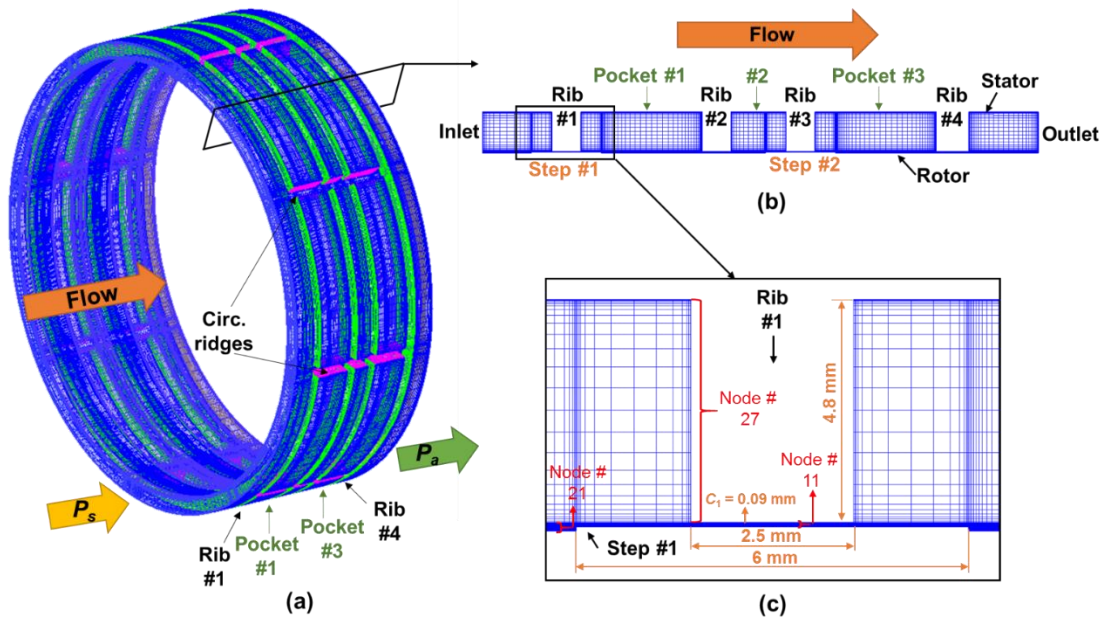


Figure 9. Three-dimensional mesh for a stepped shaft and a four-rib fully partitioned pocket damper seal assembly. (a) Three-dimensional mesh; (b) a cross section view of the mesh; and (c) mesh details around first rib and first step.

As to the CFD predictions of dynamic force coefficients for a regular PDS, an unsteady state flow model [29] implements a multi-frequency, elliptic orbit method and mesh deformation technique for rotor whirl motion with a given displacement. However, this CFD model is not adequate for a stepped shaft and seal assembly. Due to the existence of steps on rotor, the mesh near a corner deforms severely during rotor precession, thus resulting in numerical failure of the flow solver. As the two-dimensional schematic diagram in Figure 10(b) shows, the red squares near a corner on the stepped rotor, having two sides fixed on the rotor wall and the other two free to move during mesh deformation, can change shape (distort) as the rotor displaces.

Note since a PDS is not axisymmetric and the force coefficients for a gas PDS are frequency dependent, a moving coordinate transform method, as in Ref. [30], is not applicable to produce dynamic force coefficients.

To overcome the difficulties by the stepped rotor surface, a mesh separation method is presently introduced. Figure 11 displays a schematic diagram for the said method. The upper block 1 is the mesh for the seal film. The bottom block 2 includes the mesh layers near steps on rotor surface. These two blocks link to each other through interfaces. During rotor whirl, the mesh in block 2 works as rigid structure accompanying the movement of rotor wall. A transient mesh deformation happens in block 1, away from the corners on the rotor. The method transforms the mesh deformation from the rotor step towards the internal mesh. Note the mesh deformation method is applicable for the CFD analysis of seals with an irregular rotor surface, and not just limited to the present circumstance.

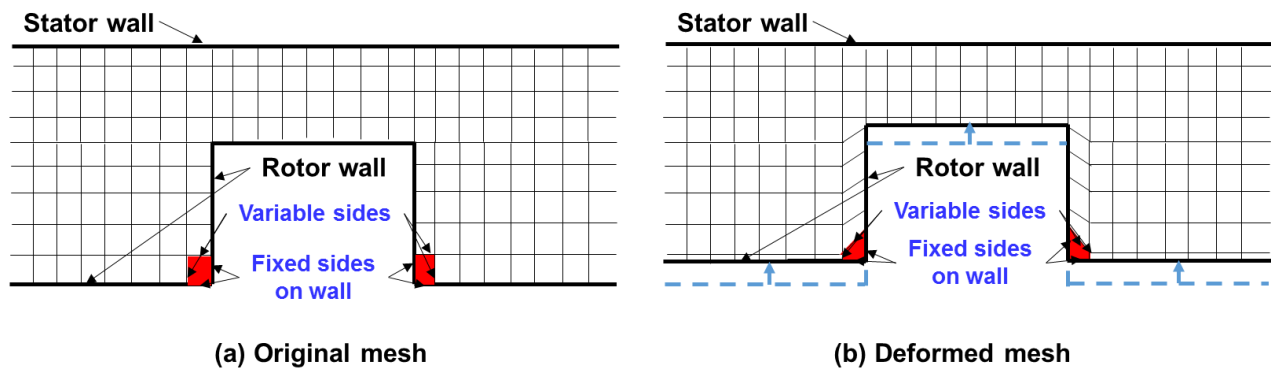


Figure 10. (a) A schematic diagram showing the mesh for a stepped rotor and a smooth seal assembly; (b) a likely severe mesh deformation at a corner of step.

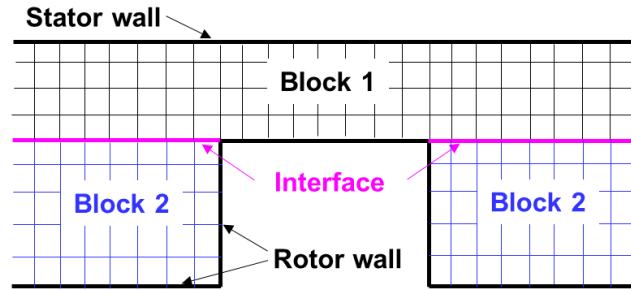


Figure 11. The mesh separation method for a stepped rotor and a smooth seal assembly (not to scale).

With the aid of the mesh deformation method, a CFD analysis implements a multi-frequency, elliptic orbit whirl method [16] to predict the seal reaction forces ( $F_X$ ,  $F_Y$ ) in the time domain. The rotor elliptic orbit is given as

$$X_{(t)} = a \sum_{j=1}^N \cos(\omega_j t); \quad Y_{(t)} = b \sum_{j=1}^N \sin(\omega_j t) \quad (1)$$

where  $(X, Y)$  represents the rotor displacements;  $\omega_j$  stands for an excitation frequency ( $j = 1, 2, \dots, N$ ); and the amplitudes  $a = 0.1 c_2/N$ ,  $b = \frac{1}{2} a$ ; and. Here,  $\{\omega_j\} = 2\pi \{10 \text{ Hz}, 20 \text{ Hz} \dots 140 \text{ Hz}\}$  ( $N = 14$ ). Figure 12 shows the rotor displacement in one rotor elliptic orbit whirl period.

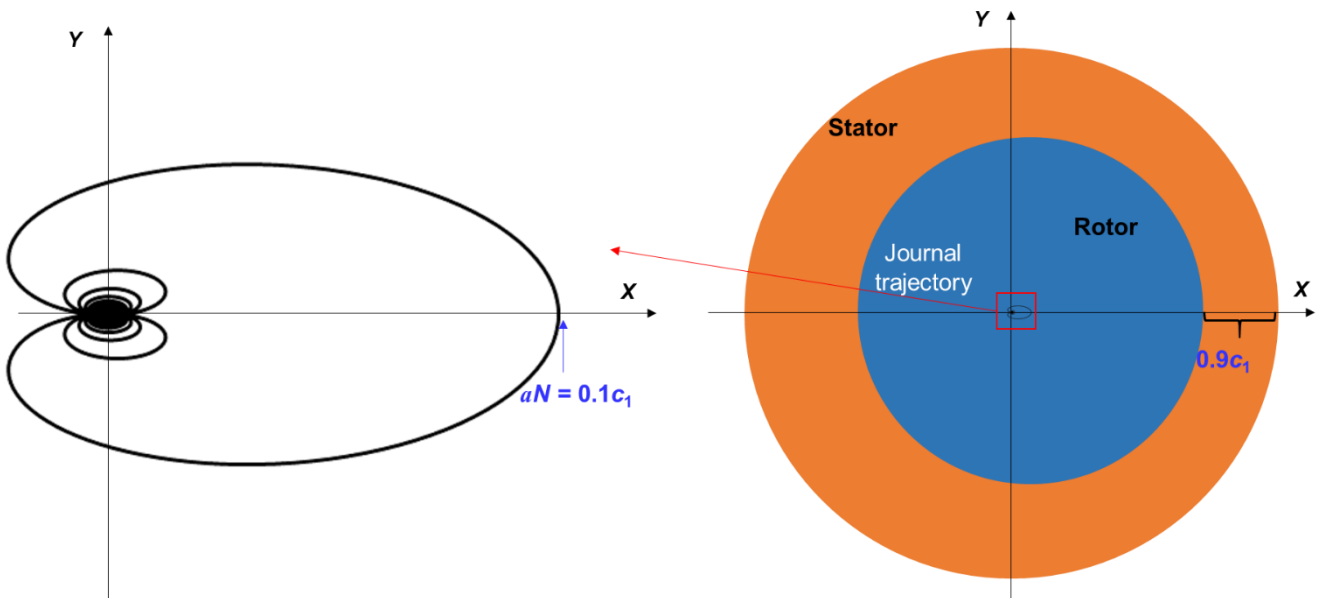


Figure 12. Rotor center displacement during one period of whirl orbit from multiple excitation frequencies.

Once completed a solution, a Discrete Fourier transformation (DFT) turns the displacements and obtained reaction forces into its frequency domain components.

$$\begin{cases} \bar{F}_{X_j} = \bar{F}_{X(\omega_j)} = \text{DFT}(F_{X(t)}) \\ \bar{F}_{Y_j} = \bar{F}_{Y(\omega_j)} = \text{DFT}(F_{Y(t)}) \end{cases}, \begin{cases} \bar{X}_j = \bar{X}_{(\omega_j)} = \text{DFT}(X_{(t)}) \rightarrow a \\ \bar{Y}_j = \bar{Y}_{(\omega_j)} = \text{DFT}(Y_{(t)}) \rightarrow ib \end{cases} \quad (2)$$

where  $(\bar{F}_{X_j}, \bar{F}_{Y_j})$  and  $(\bar{X}_j, \bar{Y}_j)$  are the reaction force and rotor displacement at frequency  $\omega_j$ , and  $i$  is the imaginary unit. The relationship between  $(\bar{F}_{X_j}, \bar{F}_{Y_j})$  and  $(\bar{X}_j, \bar{Y}_j)$  is modified as

$$-\begin{bmatrix} \bar{F}_{X_j} \\ \bar{F}_{Y_j} \end{bmatrix} = \begin{bmatrix} H_j & h_j \\ -h_j & H_j \end{bmatrix} \begin{bmatrix} \bar{X}_j \\ \bar{Y}_j \end{bmatrix} \quad (3)$$

where  $H_j$  and  $h_j$  represent the complex direct and quadrature dynamic stiffnesses. The real and imaginary parts of the complex dynamic stiffnesses are

$$H_j = H_{R_j} + i H_{I_j} \leftarrow \frac{(aF_{X_j} - ibF_{Y_j})_j}{(a^2 - b^2)}, h_j = h_{R_j} + i h_{I_j} \leftarrow \frac{(aF_{Y_j} + ibF_{X_j})_j}{(a^2 - b^2)}; j = 1, \dots, N \quad (4)$$

where subscripts  $R$  and  $I$  are the real and imaginary parts respectively. Note the formulas  $H_R = (K - \omega^2 M)$ ,  $h_R = (k - \omega^2 m)$  and  $H_I \sim (C\omega)$  are only valid for a liquid seal, with  $K$  and  $k$  as the direct and cross-coupled stiffness coefficients;  $C$  and  $c$  as the direct and cross-coupled damping coefficients; and  $M$  and  $m$  as the added mass coefficients.

In addition, a bulk flow model (PD\_Seal<sup>®</sup>)<sup>2</sup> [15] also predicts the leakage and dynamic force coefficients for both the stepped shaft and PDS assembly and the regular fully partitioned PDS under the operating conditions listed in Table 1. For the evaluation of the stepped shaft and a fully partitioned PDS assembly, the set clearances for all the four ribs along the axial direction are 0.094 mm (step #1), 0.184 mm, 0.094 mm (step #2) and 0.184 mm, respectively. Recall the bulk-flow model (BFM) analyzing a PDS was developed in 1999 by Li and San Andrés [13]; not ever revised or updated since then. Appendix A presents the graphic user interface (GUI) for PD\_Seal<sup>®</sup> and lists both input and output (I/O) results.

<sup>2</sup> Code available in XLTRC<sup>2</sup> software suite.

## 4. RESULTS AND DISCUSSION

### Static performance for a uniform clearance PDS and a stepped shaft PDS

The flow factor ( $\phi$ ) introduced by Proctor and Delgado [31] presents the seal leakage ( $\dot{m}$ ) in a way independent of seal size (diameter  $D$ ) and flow conditions (supply pressure  $P_S$  and temperature  $T_S$ ); that is,

$$\phi = \frac{\dot{m}\sqrt{T_S}}{P_S D} \quad (5)$$

Note the flow factor  $\phi$  has a physical dimension equal to  $[\text{kg}\sqrt{\text{K}}/(\text{MPa}\cdot\text{m}\cdot\text{s})]$ .

Figure 13 depicts the test derived, CFD predicted<sup>3</sup> and BFM predicted leakage ( $\dot{m}$ ) and its flow factor ( $\phi$ ) for both the stepped shaft PDS and the uniform clearance PDS versus pressure ratio ( $P_S/P_a$ ). As stated earlier, the uniform clearance PDS is the one without the steps on the rotor. Due to the limitation in the laboratory supply pressure, test data for the uniform clearance PDS operating with  $P_S > 2.1$  bar is not available as it demands more flow.

Due to the steps on the shaft (lower clearance ratio  $c_1/c_2 = 0.5$ ), the test stepped shaft PDS shows a smaller leakage than the uniform clearance PDS does. At a pressure ratio ( $P_S/P_a$ ) = 2.0,  $\phi$  for the stepped PDS is only about half of that for the uniform clearance PDS. The CFD predictions match well the test results for ( $P_S/P_a$ ) > 1.8. For the uniform clearance PDS, the BFM predicted flow factor is ~ 8% lower than the test data when ( $P_S/P_a$ ) > 1.3. While for the stepped shaft and PDS assembly, the BFM  $\phi$  agrees with the test data when ( $P_S/P_a$ ) > 1.9.

San Andrés et al. [32] produce a modified flow factor ( $\phi^*$ ) and introduce a loss coefficient ( $c_d$ ) to represent the seal effectiveness to reduce leakage.

$$\phi^* = \frac{\dot{m}\sqrt{T_S}}{P_S D \sqrt{1 - (P_a / P_S)^2}}, \quad c_d = \frac{\dot{m}\sqrt{R_g T_S}}{\pi D C_r P_S \sqrt{1 - (P_a / P_S)^2}} \quad (6)$$

where  $R_g = 287 \text{ J}/(\text{kg}\cdot\text{K})$  is the gas (air) constant, and  $C_r$  is the seal clearance. For the uniform clearance PDS,  $C_r = c_2 = 0.184 \text{ mm}$ ; for the stepped shaft PDS,  $C_r = c_1 = 0.094 \text{ mm}$ . For a detailed derivation of the two factors, refer Ref. [32].

<sup>3</sup> The CFD predicted flow factor using a finer mesh ( $5.7 \times 10^6$ ) is within 1% difference with the CFD results for the medium mesh ( $3.9 \times 10^6$ ), thus not shown here for brevity.

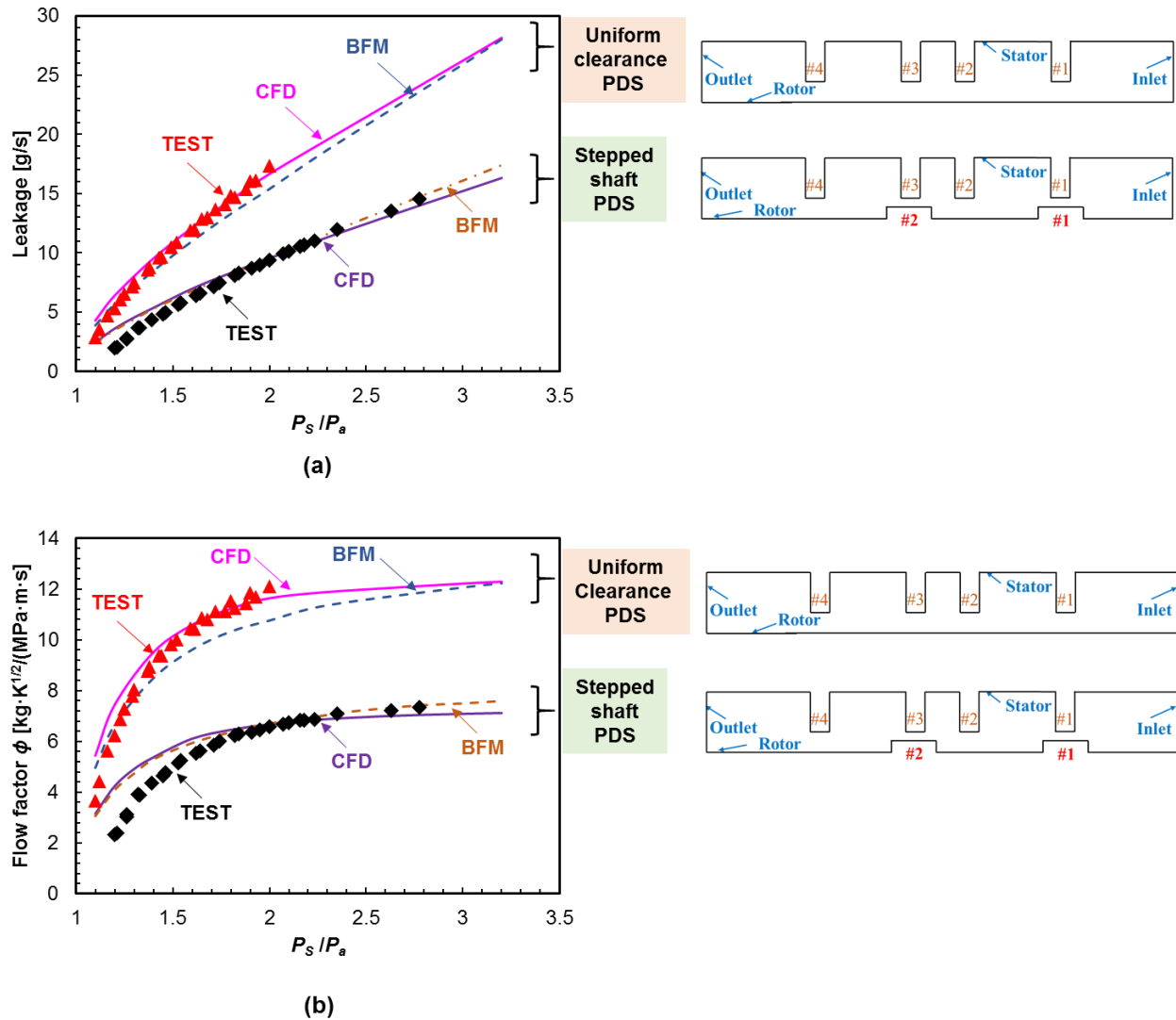


**Figure 13.** Measured, CFD predicted and BFM predicted (a) leakage [g/s]; and (b) flow factor ( $\phi$ )  $[\text{kg}\sqrt{\text{K}}/(\text{MPa}\cdot\text{m}\cdot\text{s})]$  vs. pressure ratio ( $P_s/P_a$ ) for a uniform clearance pocket damper seal (clearance ratio  $c_1/c_2 = 1$ ) and a stepped shaft pocket damper seal (clearance ratio  $c_1/c_2 = 0.5$ ). Fully partitioned pocket damper seal,  $L/D = 0.38$ ,  $c_2 = 0.184$  mm, exit pressure  $P_a = 1$  bar.

Figure 14 depicts the modified flow factor  $\phi^*$  and loss coefficient  $c_d$  versus pressure ratio ( $P_s/P_a$ ) for the two PDSs. The experimental  $\phi^*$  for the uniform clearance PDS and stepped shaft PDS achieve a constant value,  $\sim 13.6$   $[\text{kg}\sqrt{\text{K}}/(\text{MPa}\cdot\text{m}\cdot\text{s})]$  and  $\sim 7.9$   $[\text{kg}\sqrt{\text{K}}/(\text{MPa}\cdot\text{m}\cdot\text{s})]$  respectively, when  $(P_s/P_a) > 1.9$ . As to the loss coefficient,  $c_d \sim 0.45$  for the stepped shaft PDS while  $c_d \sim 0.40$  for the uniform clearance PDS for  $(P_s/P_a) > 1.9$ .

Note as  $(P_s/P_a) \rightarrow 1$ , the test derived  $c_d \rightarrow 0$  which denotes a deviation from inertial flow toward viscous dominated flow. Recall  $c_d = 1$  for an isentropic condition (inviscid fluid and adiabatic flow). The CFD and BFM predicted  $c_d$  are too large as they do not account for the flow laminarization when  $P_s/P_a < 1.5$ .

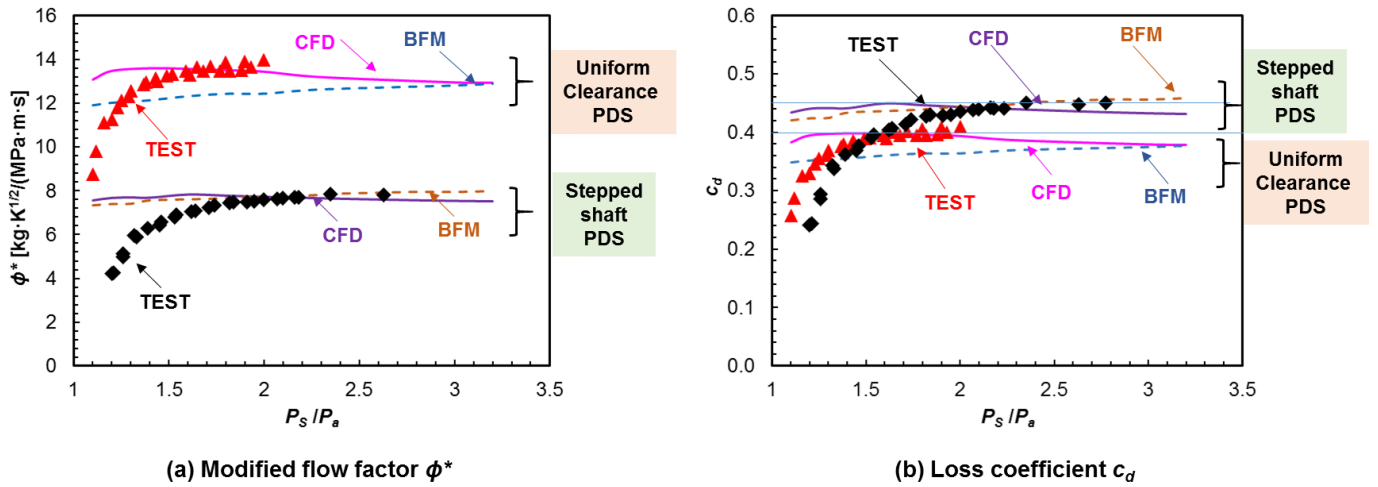


**Figure 14.** Test derived, CFD predicted and BFM predicted (a) modified flow factor ( $\phi^*$ )  $[\text{kg}\sqrt{\text{K}}/(\text{MPa}\cdot\text{m}\cdot\text{s})]$ ; and (b) loss coefficient  $c_d$  vs. pressure ratio ( $P_S/P_a$ ) for a uniform clearance pocket damper seal (clearance ratio  $c_1/c_2 = 1$ ) and a stepped shaft pocket damper seal (clearance ratio  $c_1/c_2 = 0.5$ ). Fully partitioned pocket damper seal,  $L/D = 0.38$ ,  $c_2 = 0.184$  mm, exit pressure  $P_a = 1$  bar.

Figure 15 depicts the CFD predicted and BFM predicted cross-film average static pressure ( $\bar{P} / P_a$ ) along the flow direction ( $z$ ) for the stepped shaft PDS and the regular PDS operating with supply pressure  $P_S = 2.3$  bar and 3.2 bar. For both PDSs, the average static pressure  $\bar{P}$  decreases when the air passes below a rib, while  $\bar{P}$  is almost a constant within a pocket. The CFD predicted  $\bar{P}$  for the stepped shaft PDS decreases more when the air flows below the first rib (#1) and also the third rib (#3), when in comparison to those for the regular PDS. Note the CFD predicted pressure drops below rib #2 and rib #4 for the stepped shaft PDS are lesser than those in the regular PDS. Incidentally note the pressure drop near #3 rib in the stepped shaft PDS is very large,  $\sim 1$  bar, unlike what happens in the regular PDS. The CFD predictions indicate the position of the steps on the rotor surface influences the pressure drop through the seal, which is helpful in their design. The BFM predicted  $\bar{P}$ s in the three pockets are slightly lower than the CFD predictions for both seals operating with  $P_S = 2.3$  bar and 3.2 bar, except  $\bar{P}$  for the third pocket (#3) of the stepped shaft PDS.

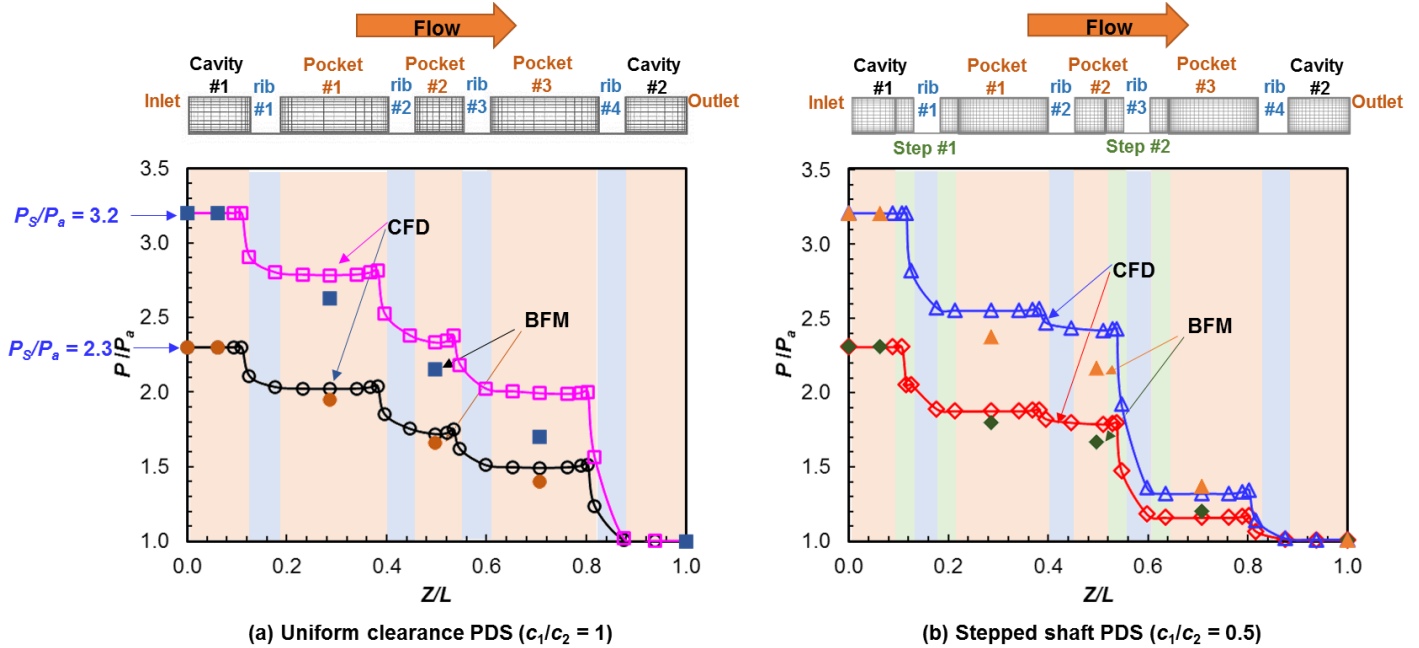


Figure 15. CFD and BFM predicted static pressure ratio ( $P/P_a$ ) vs. axial distance ( $Z/L$ ) for a uniform clearance pocket damper seal (clearance ratio  $c_1/c_2 = 1$ ) and a stepped shaft pocket damper seal (clearance ratio  $c_1/c_2 = 0.5$ ). Fully partitioned pocket damper seal,  $L/D = 0.38$ ,  $c_2 = 0.184$  mm, supply pressure  $P_s = 2.3$  bar or 3.2 bar, exit pressure  $P_a = 1$  bar.

Figure 16 and Figure 17 depict the static pressure ( $P$ ) contours on the rotor and stator surfaces of the two PDSs for operation under a supply pressure equal to 2.3 bar(a). The static pressure ( $P$ ) on the rotor of the stepped shaft PDS decreases more rapidly than that in the uniform clearance PDS, around the locations marked 1 and 3 in Figure 16(b). The static pressure contour on the stator surface for the stepped shaft PDS shows a similar trend, i.e.,  $P$  within the #1 pocket and the #3 pocket are lower than those on the regular PDS, and  $P$  within the #2 pocket is close to that for the regular seal. The static pressure contours on the rotor and stator surfaces are in accordance with those shown in Figure 15.

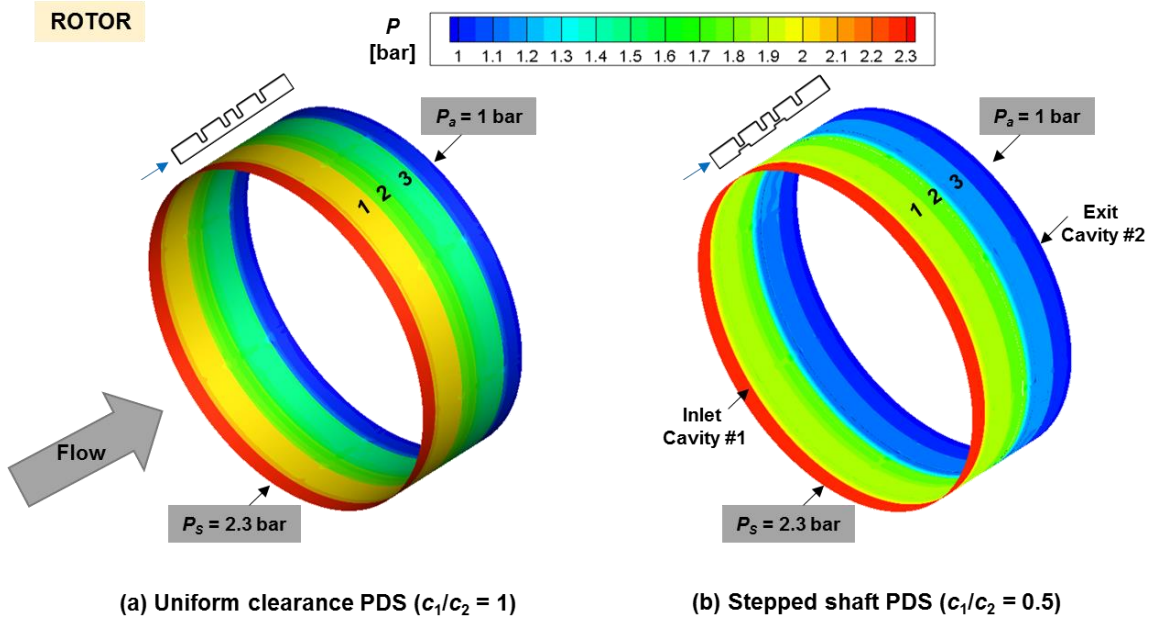


Figure 16. CFD predicted static pressure contours on rotor surface [bar] for a uniform clearance pocket damper seal (clearance ratio  $c_1/c_2 = 1$ ) and a stepped shaft pocket damper seal (clearance ratio  $c_1/c_2 = 0.5$ ). Fully-partitioned pocket damper seal,  $L/D = 0.38$ ,  $c_2 = 0.184$  mm, supply pressure  $P_s = 2.3$  bar, exit pressure  $P_a = 1$  bar.

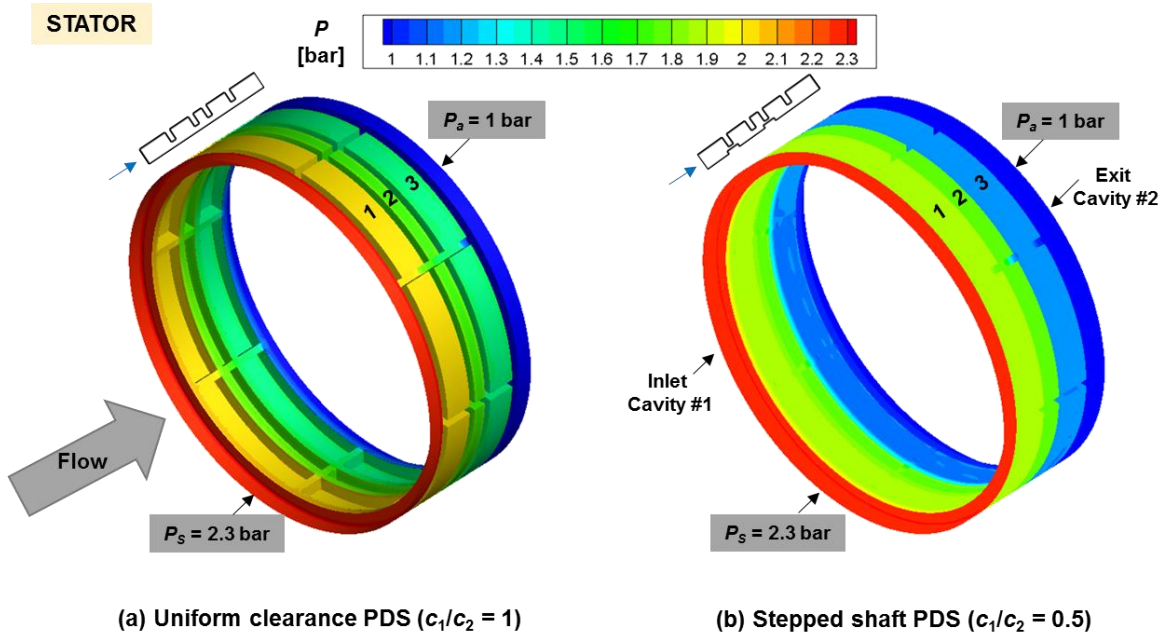


Figure 17. CFD predicted static pressure contours on stator surface [bar] for a uniform clearance pocket damper seal (clearance ratio  $c_1/c_2 = 1$ ) and a stepped shaft pocket damper seal (clearance ratio  $c_1/c_2 = 0.5$ ). Fully-partitioned pocket damper seal,  $L/D = 0.38$ ,  $c_2 = 0.184$  mm, supply pressure  $P_s = 2.3$  bar, exit pressure  $P_a = 1$  bar.

Figure 18 displays the (cross-film) average axial velocity ( $\bar{W}$ ) for the stepped shaft PDS and the uniform clearance PDS operating with supply pressure  $P_S = 2.3$  bar and 3.2 bar. For both PDSs, the average axial velocity  $\bar{W}$  increases with an increase in  $P_S$  (2.3 bar to 3.2 bar). For the regular PDS,  $\bar{W}$  increases gradually as the air passes below the ribs, from the #1 rib to the #4 rib. The maximum axial velocity  $\bar{W} = 289$  m/s for the uniform clearance PDS when supplied with  $P_S = 3.2$  bar. The high axial speed below #4 rib corresponds to the large pressure drop near the rib shown in Figure 15(a). For the stepped shaft PDS,  $\bar{W}$  for the air passing below the #1 rib is greater than that below #2 rib due to the clearance decrease ( $c_1/c_2 = 0.5$ ). The same trend is apparent for  $\bar{W}$  below the #3 and #4 ribs. The maximum  $\bar{W}$  appears when the air leaves below the #3 rib,  $\sim 226.5$  m/s for  $P_S = 3.2$  bar. The distribution of average axial velocity helps to understand the leakage decrease for the stepped shaft and PDS assembly in comparison to that for the regular PDS, as shown in Figure 13.

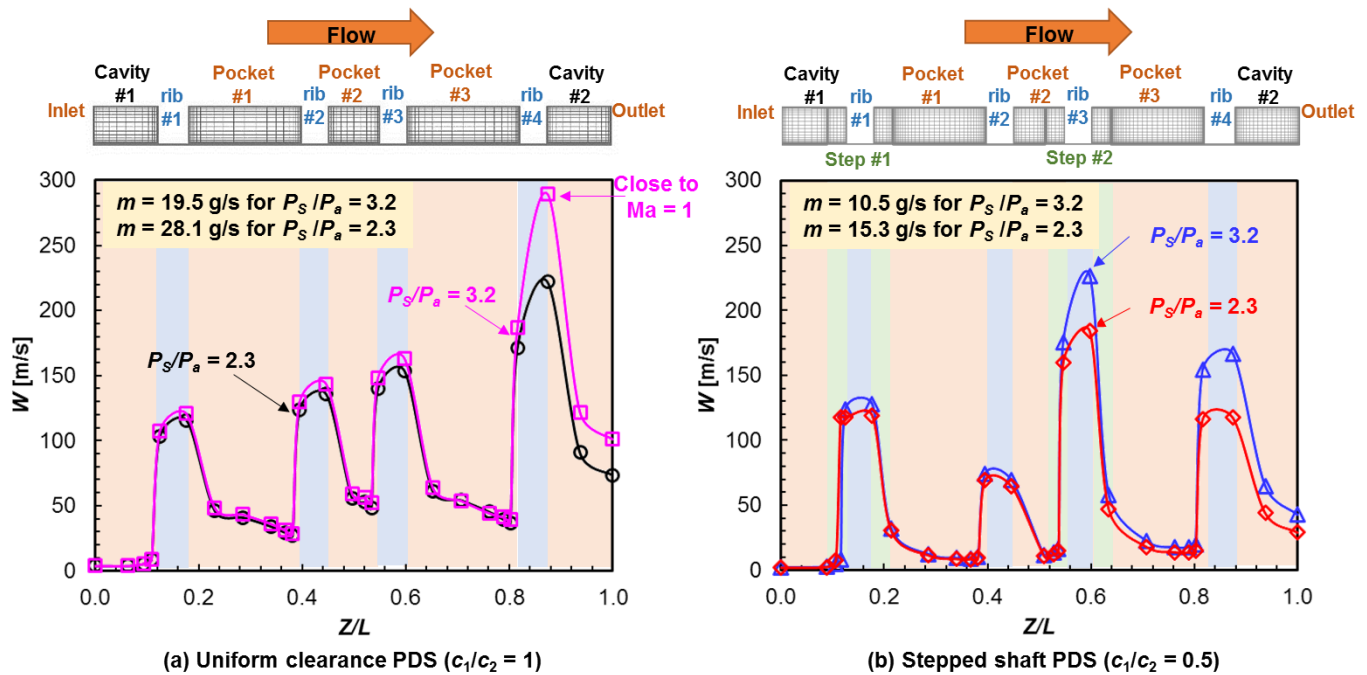


Figure 18. CFD predicted average axial velocity [m/s] along axial direction ( $Z/L$ ) for a uniform clearance pocket damper seal (clearance ratio  $c_1/c_2 = 1$ ) and a stepped shaft pocket damper seal (clearance ratio  $c_1/c_2 = 0.5$ ). Fully partitioned pocket damper seal,  $L/D = 0.38$ ,  $c_2 = 0.184$  mm, supply pressure  $P_S = 2.3$  bar or 3.2 bar, exit pressure  $P_a = 1$  bar.

### Dynamic force coefficients for a uniform clearance PDS and a stepped shaft PDS

As stated earlier, the CFD predictions for the dynamic force coefficients employ fourteen rotor excitation frequencies,  $\{\omega_j\} = 2\pi \{10 \text{ Hz}, 20 \text{ Hz} \dots 140 \text{ Hz}\}$  ( $N = 14$ ). The period for completing a rotor elliptic orbit whirl

is  $T = 0.1$ s. The time steps per rotor whirl is 500 (0.2 ms per step). The CFD analysis employs the computing resources from the High Performance Research Computing (HPRC), 40 cores per three dimensional unsteady state flow case. It takes  $\sim 32$  h CPU time to compute one period of rotor whirl motion. Typically the unsteady state flow analysis converges on the fourth period ( $4T$ ) of precession, when the differences of CFD predicted rotordynamic force coefficients (dynamic direct stiffness  $H_R$  and direct damping  $C \sim H_I/\omega$ ) from the third period and fourth period are less than 4%.

Recall the grid independence analysis between the medium size mesh (node count  $3.9 \times 10^6$ ) and a finer mesh (node count  $5.9 \times 10^6$ ) for the stepped shaft and PDS assembly. Figure 19 shows the CFD predicted direct dynamic stiffness ( $H_R$ ) and direct damping ( $C \sim H_I/\omega$ ) for the stepped shaft and PDS assembly by using these two meshes. The supply pressure equals 2.3 bar and the rotor speed is 0 rpm. For the rotor frequency ( $\omega$ ) ranging from 10 Hz to 140 Hz, the CFD predictions by using the medium mesh agree with those by using the finer mesh, thus demonstrating the medium mesh with node count  $3.9 \times 10^6$  is adequate.

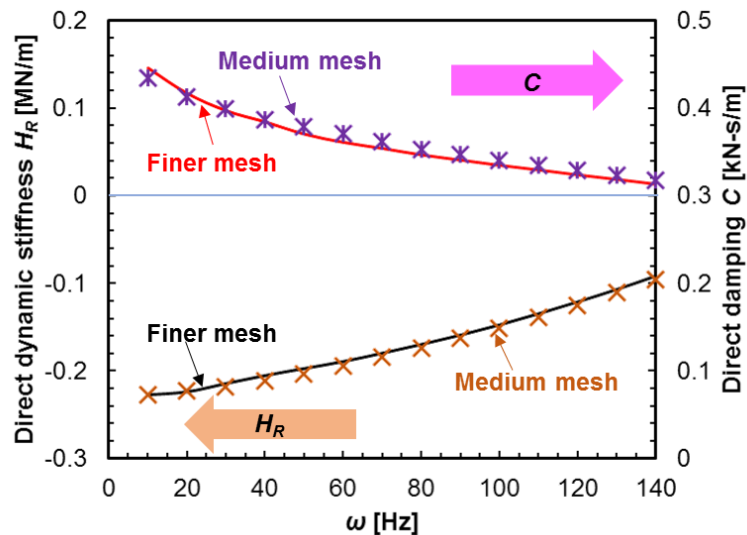


**Figure 19.** CFD predicted direct dynamic stiffness  $H_R$  and direct damping  $C$  by using a medium mesh (node count  $3.9 \times 10^6$ ) and a finer mesh (node count  $5.9 \times 10^6$ ) versus excitation frequency  $\omega$  [Hz] for a stepped shaft pocket damper seal (clearance ratio  $c_1/c_2 = 0.5$ ). Fully partitioned pocket damper seal,  $L/D = 0.38$ ,  $c_2 = 0.184$  mm, supply pressure  $P_S = 2.3$  bar, exit pressure  $P_a = 1$  bar.

Figure 20 shows the test derived, CFD predicted and BFM predicted force coefficients, namely direct dynamic stiffness ( $H_R$ ) and direct damping ( $C$ ), for the uniform clearance PDS and the stepped PDS for operation with supply pressure  $P_S = 2.3$  bar and 3.2 bar. Since the rotor speed is null, the cross-coupled dynamic stiffness ( $h_R$ )

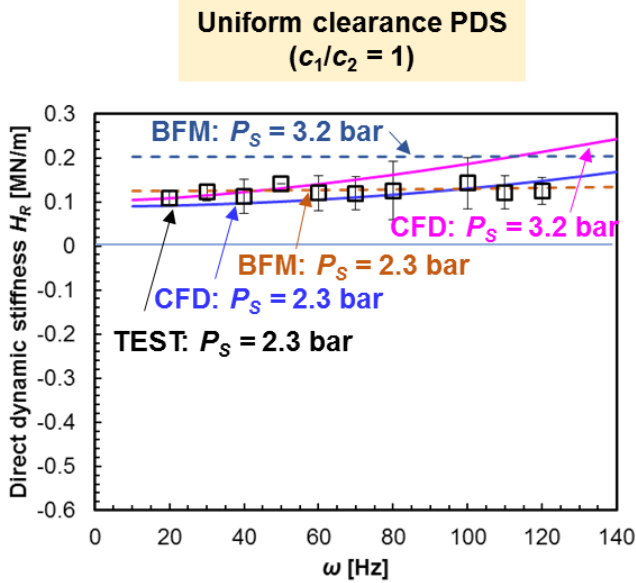
and quadrature cross-coupled stiffness ( $h_l$ ) are zero. The test results in Figure 20 are the arithmetic average of test results along the radial ( $X$ ) and tangential ( $Y$ ) directions. On these results, the error bar represents the experimental variability of the coefficients along the  $X$  and  $Y$  directions.

For the uniform clearance PDS operating with supply pressure  $P_S = 2.3$  bar, the test derived direct dynamic stiffness  $H_R$  increases slightly with an increase in the excitation frequency  $\omega$ . The test direct damping  $C$  decreases with an increase in  $\omega$ . Note that due to the limitation in the laboratory available supply pressure, test data for the uniform clearance PDS with  $P_S = 3.2$  bar is not available as it demands more flow. The CFD  $H_R$  and  $C$  match well with the test data for  $P_S = 2.3$  bar. The BFM  $H_R$  also matches well the test data. However, the BFM  $C \sim 0$  for  $P_S = 2.3$  bar and 3.2 bar, which deviates from the test data and CFD predictions.

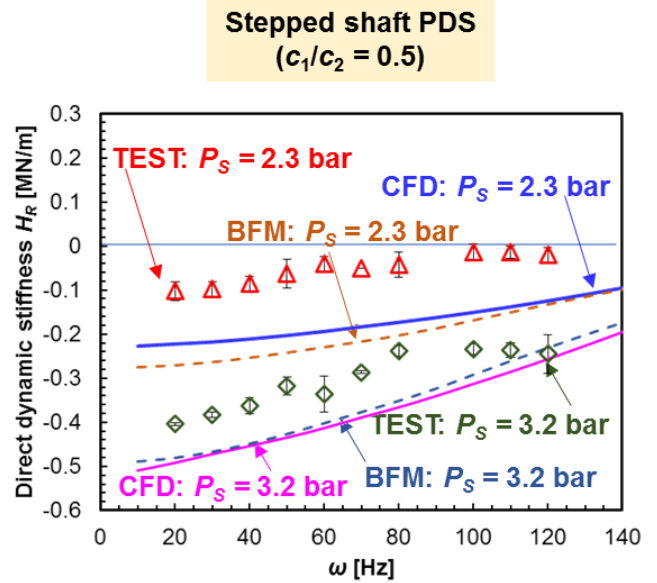
For the stepped shaft PDS, the test direct dynamic stiffness  $H_R$  is negative for both supply pressure  $P_S = 2.3$  bar and 3.2 bar.  $H_R$  decreases further with an increase in  $P_S$ . The direct damping  $C$  increases significantly when  $P_S$  increases from 2.3 bar to 3.2 bars. For instance, the test  $C$  grows from  $\sim 0.31$  kN-s/m towards 0.76 kN-s/m when  $\omega = 20$  Hz, i.e. an increase of  $\sim 2.5$  times. The variation trends of the test  $H_R$  and  $C$  versus frequency  $\omega$  are similar to those for the uniform clearance PDS. The CFD model over predicts  $H_R$  and under estimates  $C$  in comparison to the test data for both supply pressures, though showing similar variation trends vs.  $\omega$ . The BFM prediction of  $H_R$  is close to the CFD  $H_R$  for both supply pressure  $P_S = 2.3$  bar and 3.2 bar. For  $P_S = 2.3$  bar, The BFM predicted  $C$  is slightly higher than the test data and smaller than the CFD prediction. For  $P_S = 3.2$  bar, The BFM predicted  $C$  is below both the test result and the CFD prediction.

As the results in Figure 20 (a,b) show, under an identical operating condition ( $P_S = 2.3$  bar), the stepped shaft PDS and the uniform clearance PDS produce quite distinct direct stiffnesses  $H_R$ , one is negative and the other positive. Most important, the stepped shaft PDS shows a superior damping performance than the uniform clearance PDS. The test damping coefficient  $C$  for the stepped shaft PDS is  $\sim 1.5$  times larger than the one for the uniform clearance PDS when  $P_S = 2.3$  bar. When  $P_S$  increases to 3.2 bar, the stepped shaft PDS shows a more favorable damping characteristic. The CFD predicted  $C$  for the stepped shaft PDS is  $\sim 2$  times larger than the coefficient for the uniform clearance PDS.

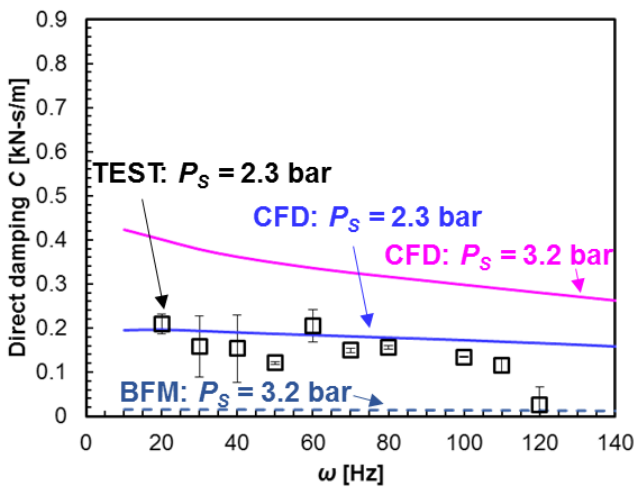
The BFM predicted dynamic force coefficients for the two PDSs, in particular the direct damping coefficient, deviate from either the test data or the CFD predictions. Recall the BFM PD\_Seal<sup>®</sup> [13] has not been updated since 1999. Hence, its update is urgent.



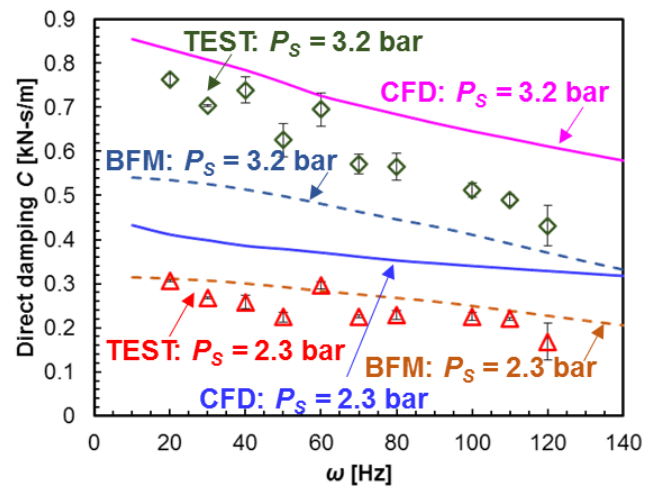
(a) Direct dynamic stiffness  $H_R$



(b) Direct dynamic stiffness  $H_R$



(c) Direct damping  $C$



(d) Direct damping  $C$

Figure 20. Test derived, CFD predicted and BFM predicted direct dynamic stiffness  $H_R$  and direct damping  $C$  versus excitation frequency  $\omega$  [Hz] for a uniform clearance pocket damper seal (clearance ratio  $c_1/c_2 = 1$ ) and a stepped shaft pocket damper seal (clearance ratio  $c_1/c_2 = 0.5$ ). Fully partitioned pocket damper seal,  $L/D = 0.38$ ,  $c_2 = 0.184$  mm, supply pressure  $P_s = 2.3$  bar or 3.2 bar, exit pressure  $P_a = 1$  bar.

## 5. CONCLUSION

Non-contact annular pressure seals limit secondary flow in compressors and gas turbines. Their dynamic force coefficients also influence the rotor bearing system stability, hence high performance turbomachinery favors seals with a large direct damping coefficient. Since their inception, pocket damper seals (PDSs) are a good choice due to their superior damping characteristics over labyrinth seals.

With more damping magnitude than that from a fully partitioned PDS, a novel stepped shaft and PDS assembly is hereby disclosed [19]. The stepped shaft PDS has a unique configuration of steps, which are below the ribs located on the upstream section of a pocket. The converging-diverging axial flow area aids to increase the damping coefficient. The stepped shaft PDS is easy to manufacture, meanwhile producing more damping and having a lesser leakage.

A stepped shaft and a four-rib, eight-pocket fully partitioned PDS assembly is built at the Turbomachinery Laboratory to test for its leakage and dynamic forced performance. There are two steps on the rotor surface, facing the first (#1) and the third (#3) ribs of the PDS. The stepped shaft PDS ( $c_1/c_2 = 0.5$ ) operates with supply pressure ( $P_S$ ) ranging from 1.1 bar to 3.2 bar and zero rotor speed. An identical fully partitioned PDS with a smooth rotor ( $c_1/c_2 = 1$ ), i.e., uniform clearance PDS, is also under investigation for performance comparisons.

The measured seal leakage for the stepped shaft PDS is much lower than that for the uniform clearance PDS,  $\sim 50\%$  less at a supply pressure/ambient pressure ( $P_S/P_a$ ) = 2.0. The CFD and BFM predicted seal leakage match well the test data when ( $P_S/P_a$ ) > 1.8. The CFD predicted static pressure contours on the rotor and stator surfaces indicate the locations of steps directly influence the pressure distribution along the axial direction.

For the uniform PDS operating with supply pressure  $P_S = 2.3$  bar, the test derived direct dynamic stiffness ( $H_R$ ) is small,  $\sim 0.1$  MN/m when rotor frequency  $\omega = 20$  Hz. The CFD and BFM predicted  $H_R$  agree with the test data. While for the stepped shaft PDS operating with  $P_S = 2.3$  bar and 3.2 bar, the test identified  $H_R$  is negative ( $< 0$ ), its magnitude enlarging with an increase in  $P_S$ . Both the CFD and BFM under-estimate  $H_R$  for the stepped shaft PDS for the two supply pressures. The BFM predicted  $H_R$  is very close to the CFD prediction.

The damping performance is the most important characteristic for a PDS. Moving from the uniform clearance PDS to the stepped shaft PDS, the test identified direct damping  $C$  increases significantly. For  $P_S = 2.3$  bar, the test derived  $C$  for the stepped shaft PDS is  $\sim 1.5$  times larger than that of the uniform clearance PDS at  $\omega = 20$  Hz. The test  $C$  for the stepped shaft PDS grows even more favorably with an increase in  $P_S$  (from 2.3 bar to 3.2 bar). Though over-predicting  $C$  for the stepped shaft PDS, the CFD predictions show similar trends versus

frequency under the given test conditions. The BFM predicted  $C$  matches well the test data at the low supply pressure ( $P_S = 2.3$  bar) for the stepped shaft PDS.

The investigation, experimental and numerical, demonstrates the superior damping performance of the invention over the uniform clearance PDS. Further work to evaluate the leakage and dynamic forced performance of the stepped shaft PDS for operation with rotor speed, distinct clearance ratios ( $c_1/c_2$ ), larger pressure drop, and under wet gas operating conditions, are planned.

## ACKNOWLEDGMENTS

The authors are grateful to the Turbomachinery Laboratory of Texas A&M University and Turbomachinery Research Consortium (TRC) for the financial supports. Thanks to the High Performance Research Computing (HPRC) in Texas A&M University for providing the computational resources, including ANSYS Fluent<sup>®</sup>. Thanks to Texas A&M Technology Commercialization for taking the idea and supporting in the application of the provisional patent [19].

## NOMENCLATURE

$c_1, c_2$	Seal radial clearances upstream and downstream a pocket [m]
$c_d$	Effective loss coefficient, $c_d = \dot{m} \sqrt{R_g T_s} / \left( \pi D C_r P_s \sqrt{1 - (P_a / P_s)^2} \right)$
$C, c$	Direct and cross-coupled damping coefficients [Ns/m]
$C_r$	Seal radial clearance [m]
$d_C$	Pocket depth [m]
$d_{step}$	Step (on rotor surface) radial height [m]
$D$	$2R$ . Rotor diameter [m]
$F_X, F_Y$	Seal reaction force components (radial and tangential) [N]
$\bar{F}_X, \bar{F}_Y$	Seal reaction force components in frequency domain [N]
$H_R, h_R$	Direct and cross-coupled dynamic stiffnesses [N/m]
$H_I, h_I$	Direct and cross-coupled quadrature stiffnesses [N/m]
$K, k$	Direct and cross-coupled stiffnesses [N/m]
$L$	Seal land length [m]
$L_C$	Pocket length [m]
$L_{step}$	Step length [m]
$\dot{m}$	Leakage (mass flow rate) [kg/s]
$P$	Static pressure [Pa]
$P_S, P_a$	Supply and discharge pressures [Pa]
$R$	Rotor radius [m]
$R_g$	Air constant, $R_g = 287$ J/(kg·K)
$T$	Period of rotor whirl [s]

$T_s$	Temperature of supply fluid [K]
$\bar{W}$	Average (cross-film) axial flow velocities[m/s]
$X, Y$	Rotor displacements in radial and tangential directions [m]
$\bar{X}, \bar{Y}$	Rotor displacements frequency domain [m]
$\delta$	Rib axial thickness [m]
$\mu$	Dynamic viscosity [Pa·s]
$\omega$	Whirl frequency [rad/s]
$\Omega$	Rotor angular velocity [rad/s]
$\phi$	Flow factor, $\phi^* = \dot{m}\sqrt{T_s} / (P_s D)$ [kg $\sqrt{K}$ /(MPa·m·s)]
$\phi^*$	Modified flow factor, $\phi^* = \dot{m}\sqrt{T_s} / (P_s D \sqrt{1 - (P_a / P_s)^2})$ [kg $\sqrt{K}$ /(MPa·m·s)]
$\rho$	Density, [kg/m <sup>3</sup> ]

### Abbreviations

BFM	Bulk flow model
CFD	Computational Fluid Dynamics
DFT	Discrete Fourier Transformation
LABY	Labyrinth seal
PDS	Pocket damper seal

### REFERENCES

- [1] Childs, D.W., and Vance, J.M., 1997, "Annular Gas Seals and Rotordynamics of Compressors and Turbines," Proc. 26th Turbomachinery Symposium, pp. 201-220.
- [2] Vance, J. M., and Schultz, R. R., 1993, "A New Damper Seal for Turbomachinery," ASME Proc. of 14<sup>th</sup> Biennial Conference on Mechanical Vibration and Noise, Vibration of Rotating Systems, **60**, pp 139-148.
- [3] Vance, J. M., and Shultz, R.R., 1993, "Modulated Pressure Damper Seals," U.S. Patent 5794942A.
- [4] Vance, J.M., and Li, J., 1996, "Test Results of a New Damper Seal in Vibration Reduction in Turbomachinery," ASME J. Eng. Gas Turb. Power, **118**(10), pp. 843-846.
- [5] Benckert, H., and Wachter, J., 1980, "Flow Induced Spring Coefficients of Labyrinth Seals for Application in Rotor Dynamics," Proc. of a Workshop on Rotordynamic Instability Problems in High-Performance Turbomachinery, Texas A&M University, College Station, TX, NASA Accession No. 80N29717, pp. 189-212. <https://ntrs.nasa.gov/search.jsp?R=19800021216>.
- [6] Ransom, D., Li, J., San Andres, L., and Vance, J. M, 1999, "Experimental Force Coefficients for a Two-Bladed Labyrinth Seal and a Four-Pocket Damper Seal," ASME J. Tribol., **121**(4), pp. 370-376.
- [7] Shultz, R.R., and Vance, J. M., 1996, "Pressure Damper Diverging Labyrinth Seals with Circumferential Partitions, and Method of Sealing," U.S. Patent 5540447.
- [8] Vance, J., M., 1998, "Modulated Pressure Damper Seal," U.S. Patent 5707064.
- [9] Ertas, B. H., Delgado, A., and Vannini, G., 2006, "Rotordynamic Force Coefficients of Pocket Damper Seals," ASME J. Turbomach., **128**(10), pp. 725-737.
- [10] Li, J., Kushner, F., and DeChoudhury, P., 2002, "Experimental Evaluation of Slotted Pocket Damper Seals on a Rotating Test Rig," ASME GT-2002-30634.

- [11] Ertas, B.H., Vance, J.M., 2007, "Rotordynamic Force Coefficients for a New Damper Seal Design," ASME J. Tribol., **129**, pp. 365-374.
- [12] Vance, J.M., Cardon, B. P., San Andrés, L., and Storage, A. F., "A Gas-Operated Bearing Damper for Turbomachinery," ASME J. Eng. Gas Turb. Power, **115**(4), pp. 383-389.
- [13] Li, J., and San Andrés, L., 1999, "A Bulk-Flow Analysis of Multiple-Pocket Gas Damper Seals," ASME J. Eng. Gas Turb. Power, **121**, pp. 355-363.
- [14] Li, J., Ransom, D., San Andrés, L., and Vance, J. M., 1999, "Comparison of Predictions with Test Results for Rotordynamic Coefficients of a Four-Pocket Gas Damper Seal," ASME J. Tribol., **121**(4), pp. 363-369.
- [15] Li, J., Aguilar, R., San Andrés, L., Vance, J. M., 2000, "Dynamic Force Coefficients of a Multiple-Blade, Multiple-Pocket Gas Damper Seal: Test Results and Predictions," ASME J. Tribol., **122**(1), pp. 317-322.
- [16] Li, J., Li, Z., and Feng, Z., 2012, "Investigations on the Rotordynamic Coefficients of Pocket Damper Seals Using the Multi-frequency, One-Dimensional, Whirling Orbit Model and RANS Solutions," ASME J. Eng. Gas Turbines Power, **134**(10), pp. 102510.
- [17] Li, Z., Li, J., and Feng, Z., 2015, "Numerical Investigations on the Leakage and Rotordynamic Characteristics of Pocket Damper Seals Part II: Effects of Partition Wall Type, Partition Wall Number, and Cavity Depth," ASME J. Eng. Gas Turbines Power, **137**(3), p. 032504.
- [18] Yang, J., San Andrés, L., and Lu, X., 2019, "Leakage and Dynamic Force Coefficients of a Pocket Damper Seal Operating Under a Wet Gas Condition: Tests VS. Predictions," ASME Paper No. GT2019-90331.
- [19] Lu, X., Yang, J., and San Andrés, L., 2018, "A stepped shaft and pocket damper seal assembly," TAMUS 4990, CR 2238-12000 (Provisional patent submitted on November 21, 2018).
- [20] Pross, J., Kramer, T., and Waltke, U., 2002, "Labyrinth Seal for Rotating Shaft," US. Patent 20020006330 A1.
- [21] Li, J., and Choudhury, P. D., 2006, "Hybrid Abradable Labyrinth Damper Seal," US. Patent 2006/0267289 A1.
- [22] Li, J., and Choudhury, P. D., 2007, "Stepped Labyrinth Damper Seal," U.S. Patent 2007/0069477 A1.
- [23] Nakaniwa, A., and Fukao, S., 2014, "Seal Device," U.S. Patent 20140175754 A1.
- [24] Gupta, M. K., Nove, S., Soulas, T., Ramesh, K., and Grosso, G., 2018, "Interlocking Hole Pattern Seal," U.S. Patent 9909440 B2.
- [25] Childs, D. W., 2013, *Turbomachinery Rotordynamics with Case Studies*, Minter Spring Pubs, 1st ed..
- [26] San Andrés, L., Lu, X., and Liu, Q., 2016, "Measurements of Flow Rate and Force Coefficients in a Short-Length Annular Seal Supplied with a Liquid/Gas Mixture (Stationary Journal)," Tribol. Trans., **59**(4), pp. 758-767.
- [27] San Andrés, L., and Lu, X., 2018, "Leakage, Drag Power and Rotordynamic Force Coefficients of an Air in Oil (Wet) Annular Seal," ASME J. Eng. Gas Turbine Power, **140**(1), pp. 012505.
- [28] ANSYS, 2016, "ANSYS Fluent User's Guide 17.2," ANSYS Inc., Canonsburg, PA.
- [29] San Andrés, L., Yang, J., and Lu, X., 2019, "On the Leakage, Torque and Dynamic Force Coefficients of an Air in Oil (Wet) Annular Seal: a CFD Analysis Anchored to Test Data," ASME J. Eng. Gas Turbines Power, **141**(2), pp. 021008.
- [30] Yang, J., and San Andrés, L., 2019, "On the Influence of the Entrance Section on the Rotordynamic Performance of a Pump Seal with Uniform Clearance: a Sharp Edge VS. a Round Inlet," ASME J. Eng. Gas Turbines Power, **141**(3), pp. 031029.
- [31] Proctor, M., and Delgado, A., 2004, "Leakage and Power Loss Test Results for Competing Turbine Engine Seals," ASME Paper No. GT2004-53935.
- [32] San Andrés, L., Wu, T., Barajas-Rivera, J., Zhang, J., and Kawashita, R., "Leakage and Cavity Pressures in an Interlocking Labyrinth Gas Seal: Measurements vs. Predictions," ASME Paper No. GT2019-91507.

## APPENDIX A: BULK-FLOW MODEL PREDICTION FOR POCKET DAMPER SEALS

It is convenient and time-efficient to employ the bulk flow model PD\_Seal<sup>®</sup> to predict the leakage and dynamic force coefficients for PDSs. The following section shows how to use the graphical user interface (GUI) of PD\_Seal<sup>®</sup> to perform the predictions for the stepped shaft PDS or uniform clearance PDS.

**Step 1:** open the PD\_Seal<sup>®</sup>, input the geometry information and operating fluid properties. Table 1 in the main text shows the information for the stepped shaft PDS. Figure 21 lists the detailed input data (geometry and fluid properties) for modeling a PDS.

**XL\_PDSEAL<sup>®</sup> LABYRINTH SEAL & POCKET DAMPER SEAL Engineering Analysis**  
 Version 1.0, Copyright 2013 by Texas A&M University. All rights reserved. Dr. Luis San Andres & Ms. Weilian Shan

Title: 4 teeth & 8 pockets FPDS (SI Units)  
 README: Color Key & Drop Down  
 PHYSICAL Units: S.I.

**Basic Geometry of Seal**

Rotor Diameter	0.127	m
Seal Outer Diameter	0.137	m
Rotor Surface Roughness	0	mm
Seal Surface Roughness	0	mm

**GAS temperature and properties**

Temperature	42	deg C
Molecular Weight	28.97	kg/kmol
Dynamic Viscosity	1.900E-05	Pa-s
Gas Compressibility Factor	1	
Specific Heat Ratio	1.4	

**Operation conditions**

Inlet Pre-Swirl Ratio	0.00
Pressure Loss Factor at Baffles	0.1

**Seal Type: Pocket Damper Seal**

# of Teeth:	4
# of Circum Pockets:	8

**update**

**Radial Baffles Parameters**

Clearance mm	Thickness mm
0.184	2.49

**Run PD\_SEAL**

**COPIE and PASTE cells:**  
 Clearance Type: "ACTIVE" or "INACTIVE"  
 Cavity Type: "LABYRINTH" or "POCKET DAMPER".

**Tooth or Blade Parameters**

	Height m	Clearance mm	C <sub>1</sub>	C <sub>2</sub>	Active/Inactive
1	0.0048135	0.094	0.35		ACTIVE
2	0.0048135	0.184	0.175		ACTIVE
3	0.0048135	0.094	0.175		ACTIVE
4	0.0048135	0.184	0.175		ACTIVE

**Axial Cavities Parameters**

	Pitch Length m	Pocket Damper / Labyrinth Cavity
1	0.01049	POCKET DAMPER
2	0.0048	POCKET DAMPER
3	0.01049	POCKET DAMPER

Figure 1 8-bladed 8 pocket FPDS with sharp teeth

Figure 21. Input of geometry and operating fluid properties in PD\_Seal<sup>®</sup>. Stepped shaft pocket damper seal (clearance ratio  $c_1/c_2 = 0.5$ ),  $L/D = 0.38$ ,  $c_2 = 0.184$  mm, supply pressure  $P_s = 2.3$  bar, exit pressure  $P_a = 1$  bar.

**Step 2:** input the seal operating conditions (supply pressure, discharge pressure, rotor speed, and excitation frequency), as shown in Figure 22.

# of test data set	17	Update		
Operating Conditions - table of inputs (speeds.txt)				
	Rotor Speed rpm	P_Supply bar	P_Discharge bar	Excitation Freq Hz
1	0	2.3	1.0	10
2	0	2.3	1.0	20
3	0	2.3	1.0	30
4	0	2.3	1.0	40
5	0	2.3	1.0	50
6	0	2.3	1.0	60
7	0	2.3	1.0	70
8	0	2.3	1.0	80
9	0	2.3	1.0	90
10	0	2.3	1.0	100
11	0	2.3	1.0	110
12	0	2.3	1.0	120
13	0	2.3	1.0	130
14	0	2.3	1.0	140
15	0	2.3	1.0	150
16	0	2.3	1.0	160
17	0	2.3	1.0	170

Figure 22. Input of operating conditions in PD\_Sea<sup>®</sup>. Stepped shaft pocket damper seal (clearance ratio  $c_1/c_2 = 0.5$ ),  $L/D = 0.38$ ,  $c_2 = 0.184$  mm, supply pressure  $P_S = 2.3$  bar, exit pressure  $P_a = 1$  bar.

**Step 3:** click the bottom, Run PD\_Sea, then all calculated results (leakage and dynamic force coefficients) appear, as shown in Figure 23.

# of test data set	17	Update			Force Coefficient								Results
Operating Conditions - table of inputs (speeds.txt)					Kxx	Kxy	Kyx	Kyy	Cxx	Cxy	Cyx	Cyy	Leakage
	Rotor Speed rpm	P_Supply bar	P_Discharge bar	Excitation Freq Hz	N/m	N/m	N/m	N/m	N-s/m	N-s/m	N-s/m	N-s/m	kg/s
1	0	2.3	1.0	10	-2.755E+05	5.983E-03	-5.983E-03	-2.755E+05	304.6	-6.6620E-06	6.6620E-06	304.6	0.0113
2	0	2.3	1.0	20	-2.714E+05	5.892E-03	-5.892E-03	-2.714E+05	302.1	-6.6070E-06	6.6070E-06	302.1	0.0113
3	0	2.3	1.0	30	-2.645E+05	5.742E-03	-5.742E-03	-2.645E+05	297.9	-6.5150E-06	6.5150E-06	297.9	0.0113
4	0	2.3	1.0	40	-2.553E+05	5.541E-03	-5.541E-03	-2.553E+05	292.1	-6.3880E-06	6.3880E-06	292.1	0.0113
5	0	2.3	1.0	50	-2.442E+05	5.298E-03	-5.298E-03	-2.442E+05	284.9	-6.2300E-06	6.2300E-06	284.9	0.0113
6	0	2.3	1.0	60	-2.318E+05	5.029E-03	-5.029E-03	-2.318E+05	276.0	-6.0350E-06	6.0350E-06	276.0	0.0113
7	0	2.3	1.0	70	-2.196E+05	4.761E-03	-4.761E-03	-2.196E+05	268.7	-5.8750E-06	5.8750E-06	268.7	0.0113
8	0	2.3	1.0	80	-2.063E+05	4.470E-03	-4.470E-03	-2.063E+05	261.4	-5.7140E-06	5.7140E-06	261.4	0.0113
9	0	2.3	1.0	90	-1.916E+05	4.149E-03	-4.149E-03	-1.916E+05	253.7	-5.5460E-06	5.5460E-06	253.7	0.0113
10	0	2.3	1.0	100	-1.739E+05	3.760E-03	-3.760E-03	-1.739E+05	245.0	-5.3530E-06	5.3530E-06	245.0	0.0113
11	0	2.3	1.0	110	-1.560E+05	3.369E-03	-3.369E-03	-1.560E+05	234.7	-5.1280E-06	5.1280E-06	234.7	0.0113
12	0	2.3	1.0	120	-1.386E+05	2.988E-03	-2.988E-03	-1.386E+05	224.3	-4.8990E-06	4.8990E-06	224.3	0.0113
13	0	2.3	1.0	130	-1.216E+05	2.616E-03	-2.616E-03	-1.216E+05	214.0	-4.6720E-06	4.6720E-06	214.0	0.0113
14	0	2.3	1.0	140	-1.049E+05	2.252E-03	-2.252E-03	-1.049E+05	203.8	-4.4490E-06	4.4490E-06	203.8	0.0113
15	0	2.3	1.0	150	-8.900E+04	1.904E-03	-1.904E-03	-8.900E+04	194.0	-4.2340E-06	4.2340E-06	194.0	0.0113
16	0	2.3	1.0	160	-7.372E+04	1.570E-03	-1.570E-03	-7.372E+04	184.6	-4.0260E-06	4.0260E-06	184.6	0.0113
17	0	2.3	1.0	170	-5.928E+04	1.254E-03	-1.254E-03	-5.928E+04	175.6	-3.8310E-06	3.8310E-06	175.6	0.0113

Figure 23. Predicted results in PD\_Sea<sup>®</sup>. Stepped shaft pocket damper seal (clearance ratio  $c_1/c_2 = 0.5$ ),  $L/D = 0.38$ ,  $c_2 = 0.184$  mm, supply pressure  $P_S = 2.3$  bar, exit pressure  $P_a = 1$  bar.

To predict the performance for the uniform clearance PDS under identical operating condition, one only needs to update the “Tooth or Blade Parameters” (shown in Figure 21) and set all the clearance as 0.184 mm. Run the code again for the BFM predictions for the uniform clearance PDS.